Bulletin of Volcanology (2026) 88:43
https://doi.org/10.1007/s00445-026-01964-y

RESEARCH

Exploring the compositional variability of magmas erupted at La Soufrière volcano, St Vincent, using chemo-stratigraphy and new $^{40}Ar/^{39}Ar$ ages

Beitris Morrison-Evans[1] · Elena Melekhova[1] · Richard Robertson[2] · Brian Jicha[3] · George Cooper[4] · Holli Frey[5] · Jonathan Blundy[1]

Received: 22 October 2025 / Revised: 14 March 2026 / Accepted: 16 March 2026

Abstract
The compositional variation of individual volcanic centres over time is key to understanding magmatic processes in the underlying crust. La Soufrière volcano, St. Vincent, Lesser Antilles, has erupted predominantly basaltic andesite magmas for hundreds of thousands of years. Sampling of the recently re-exposed crater walls at La Soufrière reveals that sequentially emplaced crater lavas, feeder dykes and lavas on the volcano's western flank are low-magnesium basaltic andesites with little variation in major and trace element concentrations. A single La Soufrière crater lava unit is more mafic (8 wt.% MgO, 51–52 wt.% SiO_2) and is compositionally similar to rare low-magnesium basaltic tephra from large explosive eruptions on St. Vincent, suggesting more primitive melts are present in the underlying crust but rarely reach the surface. New $^{40}Ar/^{39}Ar$ ages fill in a period of previously undocumented eruptive history and highlight an unconformity within the crater: a crater lava dated at 25.2 ± 3.8 ka is overlain by considerably younger lavas dated at 7.9 ± 7.7 and 5.7 ± 4.4 ka. A hornblende-gabbro xenolith is dated at 475.6 ± 28.3 ka, in agreement with early pre-Somma magmatism at La Soufrière volcano. Combining new and published data, we show that hiatuses in the geochronological record coincide with major summit collapse events and that the system appears to have stabilised compositionally after the most recent Somma collapse. The compositional uniformity of La Soufrière basaltic andesites is consistent with buffering of magma compositions by a crystal mush in the underlying crust. Commonly erupted plutonic xenoliths at St. Vincent likely represent fragments of such mushes.

Keywords La Soufrière · Crater lavas · Basaltic andesite · $^{40}Ar/^{39}Ar$ dating

Introduction

Arc volcanoes can erupt a wide range of magma types with compositional diversity observed on the scale of entire volcanic island arcs, as well as within individual volcanic centres (e.g. Lesser Antilles: Brown et al. 1977, Melekhova et al. 2015, 2017; Japan: Tatsumi et al. 1994; Kamchatka: Churikova et al. 2001, Koulakov et al. 2017). Some volcanoes, however, repeatedly generate magmas of a near-identical composition over long periods of time (e.g. thousands of years) and are thought to be chemically buffered by the composition of an underlying crustal mush source region (Hildreth and Moorbath 1988; Jackson et al., 2018; Blundy 2022). Examples of such volcanoes include Arenal, Costa Rica (Streck et al. 2002, 2005; Parat et al. 2014); North Sister, Mt. Hood, Mt. Rainier, Cascades (Schmidt and Grunder 2011; Koleszar et al. 2012; Sisson et al. 2014); Calbuco, Chile (Mixon et al. 2021); and La Soufrière, St. Vincent, Eastern Caribbean (Heath et al. 1998). The compositional monotony of these volcanoes is not always reflected in consistent eruption styles. For example, La Soufrière erupted most recently in 2020/2021, producing an effusive lava dome and subsequent explosive scoria of near-identical basaltic andesite composition (Weber et al. 2024).

Editorial responsibility: M. Edmonds

✉ Beitris Morrison-Evans
beitris.morrisonevans@earth.ox.ac.uk

[1] University of Oxford, Oxford, UK
[2] University of The West Indies, St. Augustine, Trinidad and Tobago
[3] University of Wisconsin-Madison, Madison, WI, USA
[4] Cardiff University, Cardiff, UK
[5] Union College, Schenectady, NY, USA

Published online: 28 March 2026

In this study, we explore the compositional variability of eruptive products from La Soufrière, St. Vincent, to determine how homogenous the magmatic system has been over the lifetime of the volcano. By sampling and dating a selection of newly exposed crater lavas, flank lava flows and dykes and a plutonic xenolith, we fill a gap in the dated eruptive record for La Soufrière. Using new and published geochemical and geochronologic data, we discuss La Soufrière's volcanic history in terms of processes in the underlying magma source region.

Geological setting and eruptive history

St. Vincent, located at the southern end of the Lesser Antilles volcanic island arc (Fig. 1a), is comprised of four main volcanic centres: the Southeast Volcanics field, Grand Bonhomme, Morne Garu and La Soufrière (Fig. 1b). La Soufrière is the youngest and currently active volcanic centre, dated at $\leq 0.69 \pm 0.09$ Ma (Briden et al. 1979). The oldest volcanic rocks on St. Vincent are 2.74 ± 0.11 Ma from the Southeast Volcanics complex (Briden et al. 1979) and, along with other K-Ar dates, suggest that volcanism has migrated northwards over time (Robertson 2005). Volcanism on St. Vincent is characterised by alternating periods of effusive and explosive behaviour, ranging in composition from basaltic to andesitic. Feeder dykes are identified at all volcanic centres and lava domes occur at the vents of Grand Bonhomme, Morne Garu and La Soufrière (Rowley 1978; Sigurdsson 1981; Robertson 2002).

La Soufrière volcanic deposits are divided into four main formations based on age and stratigraphy: pre-Somma lavas (PSL), Yellow Tuff Formation (YTF), Crater Lavas (CL) and Pyroclastic Formation (PF; Rowley 1978; Sigurdsson 1981; Heath et al. 1998), followed by two pre-historic (1440

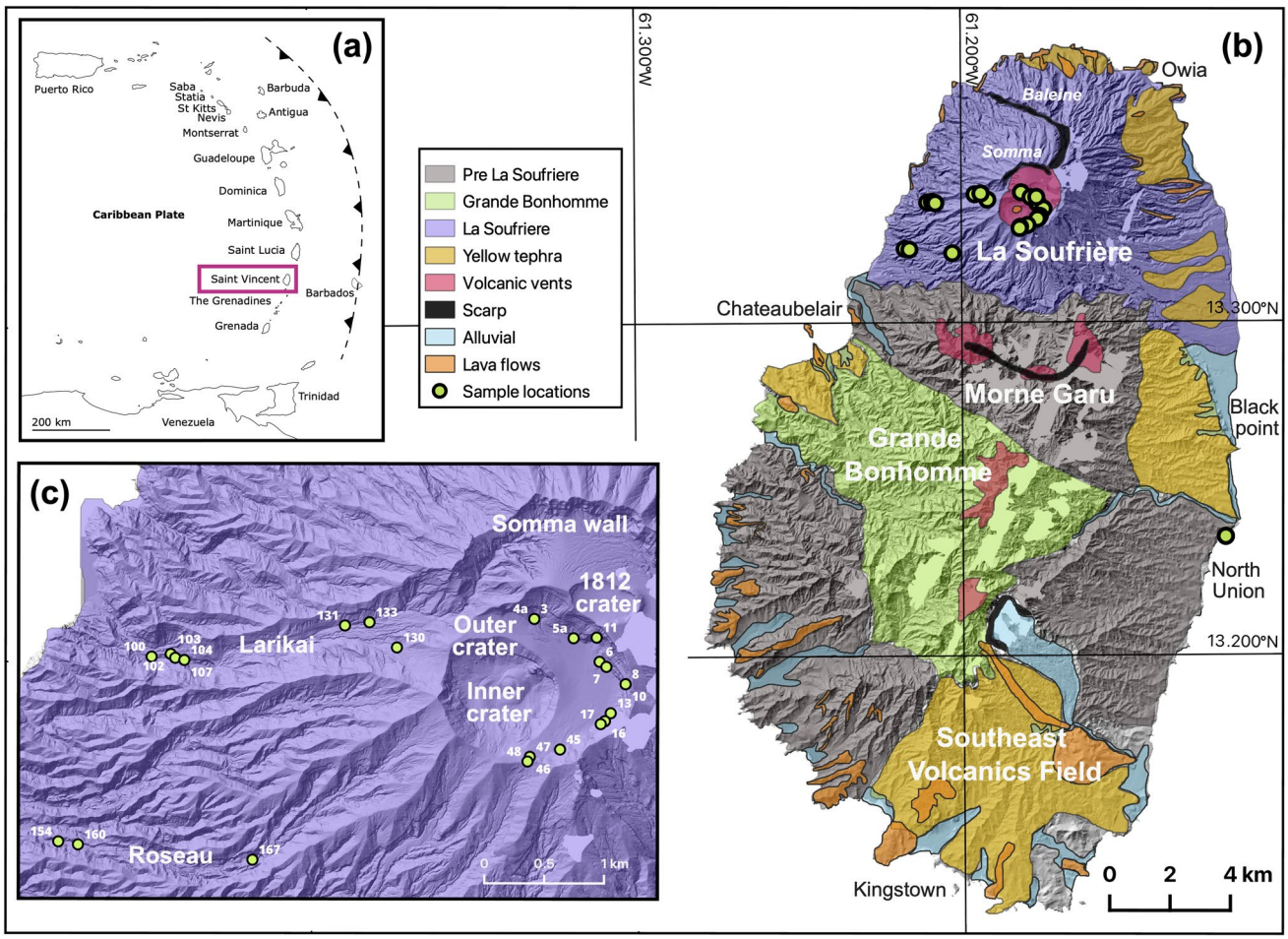

Fig. 1 Map of **a** the Lesser Antilles volcanic island arc and **b** the island of St. Vincent. The four volcanic centres present on St. Vincent are labelled, with La Soufrière being the youngest and currently active. Volcanic centres represent areas where vents have previously been identified or inferred (Robertson 2002). Geological units after Robertson (2005). Digital elevation model data from USGS-VDAP. **c** Inset map showing sample numbers and locations in La Soufrière outer crater and Larikai and Roseau valley, as listed in Table 1 (e.g. STV_LS_3 shown as number 3). Remnant Somma wall and La Soufrière craters labelled (1812, outer and inner crater)

and 1580 CE) and six major historic eruptions (1718, 1812, 1902/1903, 1971/1972, 1979 and 2020/2021 CE; Cole et al. 2019). All historic eruptions show some combination of dome-forming and/or explosive activity.

The pre-Somma lavas form the base of the La Soufrière volcano and pre-date the Somma edifice (hence the term 'pre-Somma'; Heath et al. 1998). Pre-Somma lavas are dated at 0.69 ± 0.09 Ma (K-Ar; Briden et al. 1979) to $\leq 0.18 \pm 0.02$ Ma ($^{40}Ar/^{39}Ar$; Heath 1997) and represent at least 500,000 years of effusive shield-building volcanism, with few observed intercalated pyroclastic deposits (Sigurdsson 1981). Collapse of the pre-Somma edifice is inferred by a large scarp opening to the west called the Baleine scarp (Fig. 1b). Offshore debris avalanche deposits place this flank collapse event at less than 50 ka (Le Friant et al. 2009). The Somma edifice grew subsequently to the south of the Baleine scarp before a second major collapse, this time to the southwest, evidenced by the remaining northern Somma crater wall (Fig. 1c) and voluminous debris flows to the southwest (Sigurdsson 1981). The timing of the Somma collapse is unknown, though one estimate tentatively places it at a few thousand years ago based on eruption rates and the volume of the Somma edifice (Le Friant et al. 2009).

Immediately overlying the Somma collapse debris flows are thick island-wide deposits of the Yellow Tuff Formation (YTF) which are 150 m thick in the crater and ≤ 5 m thick in Kingstown 20 km south of the crater (Rowley 1978). These deposits are poorly defined and not well constrained. Numerous 'yellow' tephra beds are identified across St. Vincent and on the flanks of La Soufrière, with only some correlated to the YTF; consequently, it is unclear whether the YTF represents a single large event or a series of closely related events. There are no age determinations for the YTF air-fall deposits, largely due to the paucity of datable material. Two pyroclastic flow deposits that *underlie* and *overlie* a thickly bedded air-fall deposit identified as part of the YTF, are radiocarbon dated at 4335 ± 95 and 3590 ± 70 years BP respectively (Rowley 1978), constraining the age of that particular fallout eruption to within a 700-year window. Rowley (1978) identified six separate YTF pyroclastic flows between 4.5 and 3.5 ka. Hay (1959) radiocarbon dated two pyroclastic flows that *overlie* a thick fallout deposit, again inferred to be the YTF, and obtained ages of 4090 ± 50 and 3890 ± 300 years BP. The air-fall deposits immediately overlying the Somma collapse debris flow deposits in the south and west walls of the crater are referred to as the Brown Tuff formation by Sigurdsson (1981), who proposes its equivalence to the YTF. The Brown Tuff demonstrably *underlies* a sequence of crater lavas in Sigurdsson's (1981) geological map.

The Crater Lavas represent the interior of the youngest and most recent La Soufrière edifice, exposed in a series of nested craters at the southern rim of the previous Somma edifice (Fig. 1c). Based on observations from the southern and western rim of the outer crater (Sigurdsson 1981), the majority of the Crater Lavas overlie and post-date the Brown Tuff (assumed equivalent to YTF by Sigurdsson), although some Crater Lavas are indicated beneath the Brown Tuff in the SSE wall of the crater close to a cross-cutting dyke and within debris flow deposits (Fig. 1 of Sigurdsson 1981). The Crater Lavas represent a period of continuous effusive volcanism (similar to the pre-Somma lavas), without visible intercalated ash layers. Activity then transitioned to alternating explosive and effusive behaviour known as the Pyroclastic Formation period, during which the current La Soufrière edifice was excavated (Fig. 1c), with the 1812 eruption forming its own crater on the NE rim of the outer crater and the inner crater forming during the 2020/2021 eruption. Today, activity continues to alternate between explosive pyroclastic density current (PDC) forming eruptions and effusive lava dome extrusions that are confined to the crater; products from both eruption types have near-identical compositions (Heath et al. 1998; Cole et al. 2019; Fedele et al. 2021; Weber et al. 2024). The most recent 2020/2021 eruption involved the extrusion of a basaltic andesite lava dome, followed by a series of explosive PDC's depositing multiple pyroclastic units (U1–U5; Cole et al. 2024) and infilling the previous crater.

In addition to volcanic rocks, another important component of St. Vincent magmatism is plutonic xenoliths and cumulates, which are abundant across the island, including at La Soufrière, and range in composition from gabbros to troctolites and hornblendites (Wager 1962; Lewis 1973; Arculus and Wills 1980; Tollan et al. 2012; Melekhova et al. 2019; Fedele et al. 2021; Brown et al. 2026). These xenoliths represent fragments of the underlying crust that were picked up by ascending magmas and erupted at the surface. As such, xenoliths represent essential end-members for reconstructing crustal compositions and the magmatic history of a volcano (e.g. Melekhova et al. 2015; 2019). St. Vincent crustal xenoliths have been found in association with both lavas and scoria. Fedele et al. (2021) identify micro-xenoliths (≤ 3 cm) in scoria deposits that have different mineralogies to previously identified plutonic xenoliths and cumulates, suggesting they are sampling a different part of the sub-volcanic plumbing system. Calc-silicate xenoliths, including calcareous hornfels, are also identified at St. Vincent and suggest magmas are sampling parts of the proto-Caribbean limestone crust (Arculus and Wills 1980; Devine and Sigurdsson 1980; Camejo-Harry et al. 2024).

Geochemical and petrological context

There are more than 300 published whole-rock analyses of volcanic rocks from La Soufrière. The greatest compositional diversity at La Soufrière occurred during early pre-Somma magmatism. Although pre-Somma magmatism is

predominantly basaltic andesite (52–57 wt.% SiO_2), a number of high-magnesium basalts (≥ 10 wt.% MgO), low-magnesium basalts (6–10 wt.% MgO) and rarer andesites (57–60 wt.% SiO_2; Rowley 1978, Heath et al. 1998) are present. The high-magnesium basalts outcrop along the coastline at the base of the volcano and are inferred to have erupted during the building of the initial volcanic edifice (Heath et al. 1998). These high-magnesium basalts match magma compositions from older volcanic centres on St. Vincent (Heath et al. 1998; Robertson 2002). Subsequent magmatism is predominantly basaltic andesite with some occurrences of low-magnesium basalts. This change in composition illustrates a general evolution in magma chemistry over time from primitive, high-magnesium basalts to basaltic andesites. Andesites are subordinate; they occur in the Somma and pre-Somma lavas, Crater Lavas, dykes and YTF, but not in the Pyroclastic Formation.

Experimental studies exploring the source of the St. Vincent high-magnesium basalts propose that these magmas are derived directly from the mantle-wedge. Two possible source conditions were proposed by Pichavant et al. (2002) depending on the original magmatic water content: 1.2 GPa, 1235 °C for 1.5 wt.% H_2O, and 1.6 GPa, 1185 °C for 4.5 wt.% H_2O. H_2O content of melt inclusions in olivines from high-magnesium basalts is in the range 2.2 to 3.5 wt.% (Bouvier et al. 2008). Oxygen fugacity is estimated to lie between NNO+1 and NNO+2.3 (Pichavant et al. 2002; Pichavant and Macdonald 2007; Melekhova et al. 2015). The high-magnesium basalts are proposed to differentiate at different depths within the crust to form low-magnesium basalts, high-aluminium basalts, basaltic andesites and andesites (Melekhova et al. 2015). Of these magmas, basaltic andesites are by far the most frequently erupted composition at La Soufrière (Rowley 1978; Heath et al. 1998), yet their origin and recurrent nature are not understood.

Lava samples from the old Somma edifice, collected by Rowley (1978) from the extant northern wall, are basaltic andesite to andesite, with the more evolved compositions interpreted as effusive lava flows that never reached the coastline. Previous sampling of crater lavas revealed predominantly basaltic andesite compositions (Rowley 1978), with a small number of andesitic lavas in the eastern wall and three andesitic dykes crosscutting the crater lavas, all of which are now buried by the 2020/2021 pyroclastic deposits. All eruption products since 1440 CE are basaltic andesite, with the exception of six low-magnesium basaltic tephra samples from the 1902/1903 eruption (Cole et al. 2019).

Previous dating of volcanic deposits at La Soufrière includes radiocarbon ages of tephra samples that extend back to ~ 5 ka (Rowley 1978; Robertson, 1992; Heath 1997; Cole et al. 2019); K-Ar and $^{40}Ar/^{39}Ar$ dating of pre-Somma lavas collected from the flanks of the volcano that range from 690 to 180 ka (Briden et al. 1979; Heath 1997; Robertson 2002); and dating of marine tephra from St. Vincent in drill cores GS-27 and EN-46 in the Grenada basin. Marine tephra were correlated to St. Vincent using geochemical fingerprinting (Carey 1992) and dates for these units calculated using sedimentation rates and the boundary defining the disappearance of planktonic foraminifera in the *Globorotalia medarii* complex at the end of the last ice age (12 ka; Sigurdsson and Carey 1981; Reid et al. 1996). The absolute ages of the Crater Lavas are currently unknown and only inferred from their stratigraphic positioning.

By exploring temporal geochemical trends in a series of sequentially emplaced effusive crater lavas at La Soufrière and in dykes and lava flows from the western flanks of the volcano, we aim to determine whether La Soufrière reflects a long-lived homogenous basaltic andesite magmatic system with little compositional variation, or whether La Soufrière magmas experience different degrees of chemical modification, such as fractionation, magma mixing or sediment assimilation. Dating a selection of these samples constrains the timing of emplacement, furthering our understanding of the eruptive history of the currently active volcanic system and how magma chemistry has evolved over time.

Methods

Fieldwork

The 2020/2021 eruption at La Soufrière exposed the previously heavily vegetated crater walls, providing a unique opportunity for sampling. The crater lavas were emplaced successively, thus preserving their relative stratigraphic sequence, which is ideal for evaluating sequential changes in geochemistry and petrology. Rowley (1978) collected rocks from low in the Crater Lava formation but was unable to reach the uppermost lava units. The 2020/2021 eruption deposited up to 100 m of ash within the crater, burying the lowermost crater lavas but providing access to the upper units (Fig. 2). In 2023, a team from the University of Oxford, University of Cardiff and the University of the West Indies sampled the Crater Lavas. Sixteen individual lava units in the northeast to southeast walls were identified (Fig. 2a), with samples collected from thirteen of these.

The YTF produced thick pyroclastic deposits with lithic-rich layers containing dense blocks of lava. Six lava blocks were collected from within a 15-m-thick deposit of the YTF exposed on the east coast, just north of North Union (Figs. 1b, 3c), to compare with the composition of the crater lavas and determine if the YTF was emplaced simultaneously to the crater lavas or if the lava blocks represent older lavas (e.g. Somma or pre-Somma lavas).

In 2024, we returned to the field to sample newly exposed lava flows and dykes on the western flanks of La Soufrière.

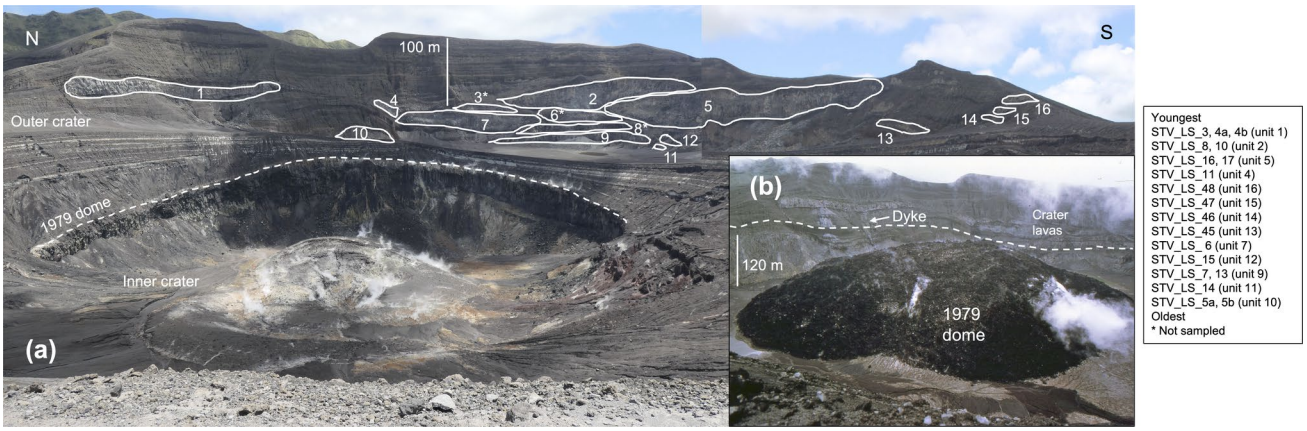

Fig. 2 **a** Photograph of La Soufrière crater lava units sampled during fieldwork in 2023. Unit numbers assigned in the field. Crater lava units ordered from youngest to oldest based on stratigraphic position. Dashed line shows upper surface of 1979 dome with radial jointing and interior now exposed. Outer crater has been historically present, with inner crater formed during the 2020/2021 eruption. **b** Photograph of the 1979 dome and lower crater lava units. Dashed line represents the floor of the outer crater today, below which is now infilled with pyroclastic material from the 2020/2021 eruption. Some lava units can be co-located, for example Unit 1, Unit 7 and the top of Unit 10 (120-m-thick coulee). Photograph **a** taken in 2023 and **b** in 1983 (by Fiske, Smithsonian Institution), both facing east

Nine lava samples and five dyke samples were collected from Larikai and Roseau valley. All sample names and locations are reported in Table 1. An adcumulate hornblende-gabbro sample (VSG-2), collected loose from Jacobs Well during a field campaign in 2009, was also dated using $^{40}Ar/^{39}Ar$ methods. This particular sample was chosen for its texture, large size and mineral assemblage, typical of xenoliths from St. Vincent (Arculus and Wills 1980).

Whole-rock geochemistry

Forty-one samples were powdered (see Appendix for details) for whole-rock major and trace element analysis using the geofacilities laboratories at the Department of Earth Sciences, University of Oxford. These samples include nineteen crater lavas, seven lava blocks recovered from the YTF, six samples from lava flows in Larikai valley, three samples from lava flows in Roseau valley, five samples from two different dykes and one sample of loose dome-rock (age unknown) collected in the current crater. Major elements were analysed by x-ray fluorescence (XRF) following a lithium-borate fusion, and trace elements were analysed by inductively coupled plasma mass spectrometry (ICP-MS) at ALS Geochemistry, Loughrea, Ireland. Precision of analyses was 2% for major elements and 10% for trace elements based on the method used. Results are reported in Tables 1 and 2.

Trace element data for the U5 scoria from the 2021 explosive eruption are also presented here for comparison. Two hundred grams of the U5 scoria was dissolved into solution and analysed using an 8900 Agilent ICP-MS at the Department of Geoscience, Union College (see Appendix for details). Major element data for these samples was previously reported in Weber et al. (2024).

$^{40}Ar/^{39}Ar$ dating

Nine lavas, a dyke and a xenolith were selected for $^{40}Ar/^{39}Ar$ dating. The criteria for the sample selection included minimal alteration and low vesicularity. Sample preparation occurred at the Department of Geoscience, University of Wisconsin-Madison. Samples were crushed, sieved and leached ultrasonically in 3 M HCl for 15 min, followed by thorough and repeated rinsing with deionised water. Purification of the groundmass by magnetic sorting and hand-picking removed phenocrysts, xenocrysts and any altered material, to leave only fresh groundmass material (180–250-µm grainsize). Samples were then loaded into aluminium foil packets and irradiated in the cadmium-lined in-core tube at the Oregon State University reactor. The 1.1864-Ma Alder Creek sanidine standard was irradiated simultaneously to monitor the neutron flux (Jicha et al. 2016).

Analysis of the irradiated samples was completed at the WiscAr Laboratory at the University of Wisconsin-Madison. Samples were incrementally heated with a CO_2 laser to release the gas trapped in the sample. The gas was then cleaned using two SAES GP50 getters (2.0 A/375°) and an Edwards Polycold cryo-cooler to remove H_2O, H_2, O_2, CO_2, CH_4 and CO. Isotopic analyses were performed on an Isotopx NGX-600 mass spectrometer operated at a trap current of 650 µA. $^{40}Ar/^{39}Ar$ ages are calculated using the decay constant from Min et al. (2000) and an atmospheric $^{40}Ar/^{36}Ar$ ratio of 298.5 ± 0.31, as determined by Lee et al. (2006). Heating steps that caused an increase in mean


3
2
7
8
9
50 m
(a)
Facing E
Facing N
4
unit 7
10
20 m
(b)
YTF
5 m
(c)
Facing W
Facing SW
Lower Larikai lava (STV_LS_103)
Debris flow
Lower Larakai dyke
5 m
Lower Larikai lava (STV_LS_104)
Debris flow
(d)
(e)
Facing NW
Dyke
Upper Larikai valley
Pyroclastic deposits
Facing E
Upper Larikai dyke
Lava flow
Shearing fractures
10 m
(f)
Roseau lava (STV_LS_167)
10 m
Debris flow
Pyroclastic deposits
(g)
Facing NW
1 m
(h)
2 cm
(i)

◂**Fig. 3** **a** Crater lavas in the eastern wall with unit numbers labelled. Lavas display lens-like morphologies and are separated by red rubbly surfaces. Jointing observed within all lava flows and shearing at the centre of thicker flows (e.g. Unit 7). Pyroclastic Formation units continue above Unit 3. Note person at foot of cliff (Unit 9) for scale. **b** Crater lavas in northeastern wall. Top of Unit 10 exposed and covered in thick pyroclastic deposits. Unit 4 is a considerably younger upper crater lava emplaced ≤ 30 m above Unit 10. **c** 15-m-thick YTF deposit displaying layering and containing large lithic lava blocks (≤ 70 cm) near North Union (see Fig. 1b). **d** Lava flows in lower Larikai valley interbedded with debris flows and crosscut by a vertical dyke. **e** Upper Larikai valley with a dyke exposed on the northern side of the valley (circled). Lavas in the background covered by vegetation are likely the Somma lavas comprising the still standing northern Somma crater wall. Thick pyroclastic deposits in the valley make access to lavas difficult. **f** Contact between Upper Larikai dyke and lava flow. Upward tilt of lava flow and shearing fractures at the base of the exposure clearly observed. **g** Thick lava flow in Roseau valley (STV_LS_167) with sheared interior exposed. **h** Giant xenolith block from Roseau valley predominantly composed of interlocking plagioclase, clinopyroxene and olivine crystals. Clusters of different mineral assemblages observed, some displaying layering and banding (circled). **i** In situ micro-xenolith (≤ 3 cm) in lower Larikai lava STV_LS_100. It contains plagioclase and olivine and displays a recrystallised darker core

standard weight deviation (MSWD) ≥ 1.5 were excluded from the calculated ages (Powell et al. 2002; Jicha et al. 2016) and are shown in the plateau diagrams in the supplementary material (Fig. S1). The inverse isochrons all have intercepts that are within uncertainty of the atmospheric value, indicating that excess Ar is not present. Therefore, the plateau ages reported in Table 3 are used in the subsequent discussion.

Results

Field observations

The exposed eastern wall of the crater consists of a 200-m high section through a series of jointed lava flows with lens-like morphologies separated by red rubbly surfaces corresponding to flow tops (Fig. 2a). Individual lava flows can be clearly distinguished and, where accessible, sampled. The crater wall, with identified and sampled lava units, is shown in Fig. 2a alongside a photograph of the same section taken in 1983 (Fig. 2b) when the 1979 lava dome was still steaming. Little of the 1979 dome remains today. Several features can be correlated between the two photographs (a) and (b), including the prominent Unit 1 in the northern crater wall and a series of vertical fractures above Unit 4. Unit 10 with its curved upper surface is also evident in the 1983 photograph. This unit can also be identified in Sigurdsson's 1981 map of the crater, where it is labelled as a 'pre-historic coulee' and 'coulee flow front'. Our field observations confirm the sequential emplacement of the Crater Lavas (e.g. filling of topographic lows, lack of well-defined interstitial ash layers), with thicker units displaying shearing (Fig. 3a). The relative age order of the Crater Lavas and their corresponding sample numbers are presented in Figs. 2 and 4. Note that it was not possible to sample three of the units, shown with asterisks in Fig. 2. The top of the crater wall comprises deposits of the Pyroclastic Formation. The Brown Tuff (YTF equivalent) identified by Sigurdsson (1981) is not present in the studied crater wall section, in keeping with his map of the crater.

The lava flows in Larikai and Roseau valleys are often extensive, interbedded with debris flows, and display shearing in thicker flows (Fig. 3g). A 15-m-tall and 10-m-wide dyke was identified crosscutting the lower Larikai lavas (Lower Larikai (LL) dyke; Fig. 3d), and a 15-m-tall, 70-m-long dyke striking 300° outcropped to the NW of the crater in the upper Larikai valley, intersecting the Somma crater wall (Upper Larikai (UL) dyke; Fig. 3e). The Crater Lavas and lava flows in Larikai and Roseau valleys contained abundant igneous and calc-silicate xenoliths (e.g. Fig. 3i); a large multi-textural xenolith block was identified in Roseau valley (Fig. 3h). Both of the sampled lavas in the lower Larikai valley immediately overlie debris flows, as does the youngest lava flow sampled in the Roseau valley. Schematic stratigraphic logs of the Larikai and Roseau valley sections are shown in Fig. 4.

Whole-rock major element chemistry

New whole-rock major element data are reported in Table 1. Compositions range from basalt to andesite (49.5–57.5 wt.% SiO_2), with most lavas sitting within the basaltic andesite field (Fig. 5). Three crater lava samples from Units 9 (STV_LS_7 and STV_LS_13) and 11 (STV_LS_14) have considerably higher magnesium (~ 8 wt.% MgO) and lower silica (~ 51–52 wt.% SiO_2) contents (Fig. 6a) and are similar in composition to previously identified low-magnesium basalts (Robertson 2002). Due to the similar composition and stratigraphic positioning of Units 9 and 11 (and their correlation to one continuous crater lava unit in Sigurdsson's 1981 map), these units are hereafter combined and referred to as the Mafic Crater Lava. The YTF lava blocks are distinctive with lower SiO_2 and NaO_2 and higher CaO and Al_2O_3 contents than the main cluster of whole-rock data (Fig. 6).

The new lava compositions presented in this study are all calcium- and aluminium-rich (~ 8–11 wt.% CaO; ~ 17–20 wt.% Al_2O_3; Fig. 6b, c), characteristic of the southern Lesser Antilles arc (e.g. Macdonald et al. 2000). K_2O contents of La Soufriere magmas are consistently low (below 0.7 wt.%) which has implications for Ar-Ar dating (see below). New data follow typical differentiation trends and are in good agreement with previous whole-rock data for La Soufrière and older St. Vincent volcanic centres. With the exception

Table 1 Whole-rock major element data

Sample #	Unit	Latitude	Longitude	SiO_2	TiO_2	Al_2O_3	FeO^T	MnO	MgO	CaO	Na_2O	K_2O	P_2O_5	Total	LOI
2023 fieldwork															
STV_LS_3	CL-1	13°20.3333′ N	61°10.9004′ W	54.79	0.89	18.91	7.89	0.18	4.24	9.01	3.39	0.54	0.13	99.97	−0.35
STV_LS_4a	CL-1	13°20.3334′ N	61°10.9005′ W	55.20	0.98	18.32	8.13	0.19	3.93	8.45	3.62	0.60	0.14	99.56	−0.20
STV_LS_4b	CL-1	13°20.3334′ N	61°10.9005′ W	56.03	0.98	18.28	8.09	0.19	3.91	8.45	3.63	0.59	0.14	100.29	−0.33
STV_LS_5a	CL-10	13°20.2465′ N	61°10.7236′ W	55.80	0.89	18.08	7.61	0.18	4.26	8.35	3.47	0.62	0.13	99.39	−0.19
STV_LS_5b	CL-10	13°20.2465′ N	61°10.7236′ W	56.22	0.88	18.10	7.50	0.18	4.12	8.28	3.53	0.62	0.13	99.56	−0.23
STV_LS_6	CL-7	13°20.1406′ N	61°10.6068′ W	54.99	0.93	18.86	7.63	0.17	4.52	8.97	3.40	0.59	0.13	100.19	−0.39
STV_LS_7	CL-9*	13°20.1175′ N	61°10.5764′ W	50.81	0.86	16.87	8.04	0.17	8.72	10.10	2.70	0.41	0.10	98.78	−0.26
STV_LS_8	CL-2	13°20.0397′ N	61°10.49′ W	55.49	0.92	18.55	7.73	0.18	4.32	8.67	3.42	0.59	0.13	100.00	−0.36
STV_LS_10	CL-2	13°20.0397′ N	61°10.49′ W	55.26	0.91	18.54	7.65	0.18	4.28	8.65	3.39	0.59	0.13	99.58	−0.39
STV_LS_11	CL-4	13°20.2497′ N	61°10.62′ W	54.63	0.93	19.04	7.69	0.17	4.74	9.28	3.46	0.59	0.12	100.65	−0.29
STV_LS_13	CL-9*	13°19.9089′ N	61°10.5567′ W	51.69	0.88	17.06	8.05	0.17	8.46	10.05	2.78	0.45	0.10	99.69	−0.28
STV_LS_14	CL-11*	13°19.8725′ N	61°10.5830′ W	52.18	0.89	17.26	8.02	0.17	7.75	9.83	2.87	0.48	0.10	99.55	−0.18
STV_LS_15	CL-12	13°19.8725′ N	61°10.5830′ W	55.99	0.78	18.68	7.35	0.19	3.44	8.43	3.43	0.55	0.14	98.98	−0.32
STV_LS_16	CL-5	13°19.8725′ N	61°10.5830′ W	57.34	0.95	17.76	7.43	0.18	3.47	7.60	3.88	0.69	0.15	99.45	−0.33
STV_LS_17	CL-5	13°19.8596′ N	61°10.6014′ W	57.25	0.94	17.74	7.40	0.18	3.45	7.57	3.91	0.69	0.15	99.28	−0.36
STV_LS_45	CL-13	13°19.7451′ N	61°10.7844′ W	55.57	0.96	18.09	8.76	0.21	3.77	8.21	3.65	0.57	0.15	99.94	−0.10
STV_LS_46	CL-14	13°19.7120′ N	61°10.9211′ W	51.74	1.02	18.92	9.10	0.20	4.78	9.91	3.26	0.45	0.12	99.50	−0.41
STV_LS_47	CL-15	13°19.7120′ N	61°10.9211′ W	51.45	1.02	18.87	9.11	0.20	4.79	9.86	3.23	0.45	0.11	99.09	−0.40
STV_LS_48	CL-16	13°19.6909′ N	61°10.9311′ W	54.23	0.79	20.29	7.23	0.17	4.02	9.59	3.34	0.55	0.12	100.33	−0.33
STV_LS_18	Dome			55.27	0.98	18.34	8.09	0.19	3.87	8.46	3.59	0.60	0.14	99.53	−0.36
STV_LS_20	YTF	13°13.7491′ N	61°07.4935′ W	50.62	0.94	19.56	8.54	0.17	5.28	10.55	2.87	0.35	0.10	98.98	0.02
STV_LS_21	YTF	13°14.1291′ N	61°07.1822′ W	49.44	1.12	20.25	8.94	0.16	5.21	11.25	2.65	0.46	0.08	99.56	0.15
STV_LS_22	YTF	13°14.1291′ N	61°07.1822′ W	55.15	0.86	18.34	8.28	0.20	3.72	8.00	3.56	0.46	0.15	98.72	0.31
STV_LS_24	YTF	13°14.1291′ N	61°07.1822′ W	53.62	0.96	19.12	7.80	0.18	3.97	8.30	3.44	0.44	0.14	97.97	0.65
STV_LS_25	YTF	13°14.1291′ N	61°07.1822′ W	51.83	0.91	20.25	8.06	0.18	4.77	10.15	2.98	0.37	0.11	99.61	−0.21
STV_LS_26	YTF	13°14.1291′ N	61°07.1822′ W	49.49	1.11	19.82	9.02	0.16	5.72	11.40	2.65	0.46	0.08	99.91	−0.25
STV_LS_27	YTF	13°18.2537′ N	61°07.7505′ W	52.03	0.91	19.48	7.95	0.17	5.49	9.71	3.02	0.42	0.12	99.30	0.31
2024 fieldwork															
STV_LS_100	LL lava	13°20.1612′ N	61°12.6243′ W	54.40	0.91	18.14	7.72	0.17	5.24	8.93	3.29	0.59	0.13	99.52	−0.16
STV_LS_102	LL lava	13°20.1735′ N	61°12.5384′ W	53.79	0.89	17.90	7.65	0.17	5.25	8.82	3.25	0.57	0.12	98.41	−0.21
STV_LS_103	LL lava	13°20.1562′ N	61°12.5178′ W	53.46	0.88	17.82	7.57	0.17	5.17	8.81	3.23	0.57	0.12	97.80	−0.07
STV_LS_104	LL lava	13°20.1464′ N	61°12.4771′ W	53.66	0.89	17.92	7.68	0.17	5.29	8.90	3.24	0.57	0.12	98.44	−0.33
STV_LS_130	UL lava	13°20.2040′ N	61°11.5197′ W	54.27	0.88	18.00	7.69	0.17	5.13	8.90	3.27	0.60	0.13	99.04	0.10
STV_LS_131	UL lava	13°20.3032′ N	61°11.7534′ W	55.32	0.91	18.43	7.80	0.18	5.15	8.98	3.30	0.60	0.13	100.80	−0.10
STV_LS_154	Roseau lava	13°19.3280′ N	61°13.0440′ W	55.34	0.90	17.80	7.94	0.18	4.42	8.15	3.57	0.70	0.14	99.14	−0.21

Table 1 (continued)

Sample #	Unit	Latitude	Longitude	SiO_2	TiO_2	Al_2O_3	FeO^T	MnO	MgO	CaO	Na_2O	K_2O	P_2O_5	Total	LOI
STV_LS_160	Roseau lava	13°19.3144′ N	61°12.9554′ W	55.12	0.90	17.61	7.87	0.18	4.39	8.07	3.51	0.70	0.14	98.49	−0.27
STV_LS_167	Roseau lava	13°19.2466′ N	61°12.1695′ W	54.21	0.97	18.22	8.78	0.21	3.98	8.97	3.40	0.50	0.13	99.37	−0.42
STV_LS_106	LL dyke—core	13°20.1464′ N	61°12.4771′ W	56.29	0.93	18.05	7.86	0.18	3.71	8.12	3.74	0.72	0.14	99.74	−0.19
STV_LS_107	LL dyke—edge	13°20.1464′ N	61°12.4771′ W	55.96	0.93	17.92	7.87	0.19	3.76	8.07	3.68	0.74	0.14	99.26	−0.02
STV_LS_132	UL dyke	13°20.3174′ N	61°11.6433′ W	56.84	0.97	17.64	8.31	0.21	3.46	7.76	3.79	0.60	0.14	99.72	−0.46
STV_LS_133	UL dyke	13°20.3174′ N	61°11.6433′ W	55.85	0.96	17.34	8.36	0.21	3.54	7.80	3.76	0.59	0.14	98.55	−0.39
STV_LS_134	UL dyke	13°20.3174′ N	61°11.6433′ W	56.87	0.93	17.56	8.11	0.21	3.46	7.80	3.83	0.62	0.14	99.53	−0.40

Latitude and longitude data in decimal degrees minutes

of the YTF lava blocks and the Mafic Crater Lava, there is no discernible chemical difference between the rock types sampled in this study, although the dykes are displaced consistently to the low-MgO end of the cluster. Melt inclusions, representing trapped droplets of liquids formed during differentiation and crystallisation, extend the chemical range of the whole-rocks, with a noticeable deviation above 7 wt.% MgO to low SiO_2, high CaO and TiO_2 and pronounced scatter at low MgO, particularly for alkalis and TiO_2. Note that many melt inclusions have compositions unmatched by any lavas on St. Vincent.

Whole-rock trace element geochemistry

Trace element concentrations and trace element ratios are reported in Table 2. Trace element concentrations are enriched by approximately one order of magnitude relative to the primitive mantle (Sun and McDonough 1989). Primitive mantle normalised rare earth element (REE), Sr, Zr and Hf patterns are relatively flat with little variation between lava samples and previous St. Vincent data (grey shading, Fig. 7). The Mafic Crater Lava generally has the lowest REE concentrations consistent with its more primitive nature. All rocks have a positive Sr anomaly (~200–250 ppm Sr; Fig. 7, Table 2) despite a small negative Eu anomaly, characteristic of arc magmas (Turner and Langmuir 2022). The magnitude of the positive Sr anomaly decreases with increasing differentiation, indicating that high Sr is an inherited feature of the parental magmas, becoming reduced during differentiation through plagioclase fractionation. Two of the YTF lava blocks display significantly higher Sr peaks (460 ppm Sr; STV_LS_21 and 26) and depletions in LREE (La-Sm) and Zr relative to other samples; these are the same lava blocks with elevated Ca and Al contents, features consistent with plagioclase accumulation.

Eu/Eu* ratios (where $Eu^* = Eu_N/\sqrt{Gd_N * Sm_N}$) for the La Soufrière magmas range from 0.8 to 1 (Fig. 8a) and decrease slightly with differentiation, as illustrated by increasing incompatible element La. The weak negative Eu anomaly observed in all new data (Fig. 7) is indicative of a low proportion of Eu^{2+} partitioning into plagioclase and therefore a higher magmatic oxidation state (Aigner-Torres et al 2007). Elevated fO_2 can account for the observed decoupling of Sr, whose positive anomaly becomes significantly less pronounced during differentiation (Fig. 7), and Eu. For example, at the redox conditions of La Soufrière magmas (≥ NNO + 1) less than 10% of Eu is divalent and hence the ratio of D_{Eu}/D_{Sr} in plagioclase is < 0.1 (Aigner-Torres et al. 2007).

The Dy/Dy* ratio (where $Dy^* = Dy_N/\sqrt{Gd_N^{4/13} * Sm_N^{9/13}}$; Davidson et al. 2013) is used to distinguish between garnet fractionation, which

Table 2 Whole-rock trace element data and key ratios

Sample #	Unit	Cs	Rb	Ba	Th	U	Nb	Ta	La	Ce	Pr	Sr	Nd	Zr	Hf	Sm	Eu	Gd	Tb	Dy	Ho
		ppm	ppm	ppm	ppm	ppm	ppm	ppm	ppm	ppm	ppm	ppm	ppm	ppm	ppm	ppm	ppm	ppm	ppm	ppm	ppm
2023 fieldwork																					
STV_LS_3	CL-1	0.17	11.5	121.5	1.12	0.58	2.62		5.4	13.6	2.07	228	10.1	83	2.39	2.67	1.01	3.7	0.62	4.27	0.86
STV_LS_4a	CL-1	0.56	14.3	128	1.14	0.6	2.95	0.8	6	14.6	2.29	225	11.4	87	2.67	3.52	1.11	4.1	0.74	5.15	1.11
STV_LS_4b	CL-1	0.52	13.8	128.5	1.2	0.61	3.06	0.2	5.7	15	2.39	230	11.5	92	2.75	3.74	1.1	4.22	0.74	4.82	1.06
STV_LS_5a	CL-10	0.18	14.4	133.5	1.17	0.6	2.8	1.3	5.8	15	2.3	230	10.8	91	2.46	3.19	0.89	3.55	0.66	4.05	0.95
STV_LS_5b	CL-10	0.15	13.7	132.5	1.2	0.64	2.71	0.2	5.9	14.7	2.2	226	10.4	89	2.71	3.08	1.08	3.89	0.67	4.12	0.99
STV_LS_6	CL-7	0.19	12.9	128	1.19	0.64	3.14	0.2	5.6	14.4	2.21	233	10.3	86	2.65	3.32	1.06	3.6	0.58	4.17	0.88
STV_LS_7	CL-9*	0.19	6.2	93.4	1.08	0.44	2.17	0.7	4.5	11.4	1.66	227	8.8	64	1.94	2.38	0.9	3.21	0.55	3.53	0.79
STV_LS_8	CL-2	0.21	13.3	129	1.18	0.58	2.91	0.4	5.6	14.3	2.13	233	10.9	86	2.57	3.03	0.97	3.8	0.64	4.37	0.99
STV_LS_10	CL-2	0.23	14	126	1.14	0.57	2.86	0.1	5.6	13.9	2.22	224	10.4	87	2.45	3.14	0.99	3.64	0.63	4.54	0.93
STV_LS_11	CL-4	0.15	13.4	122	1.15	0.59	3	0.4	5.5	14.2	2.1	233	9.9	83	2.45	2.91	1.04	3.53	0.62	4.11	0.95
STV_LS_13	CL-9*	0.3	10.7	94	0.88	0.38	2.13		4.4	11	1.69	216	8.1	65	1.9	2.38	0.81	3.13	0.49	3.51	0.73
STV_LS_14	CL-11*	0.37	11.2	102	0.94	0.47	2.18	0.3	4.6	11.5	1.82	217	9.2	69	2.14	2.58	0.9	3.12	0.58	3.83	0.76
STV_LS_15	CL-12	0.33	12.5	121.5	0.9	0.54	2.68	0.1	5.2	13.6	2.21	231	10.3	88	2.47	3.02	0.96	3.61	0.63	4.59	0.94
STV_LS_16	CL-5	0.22	15.2	148	1.4	0.67	3.3	0.4	6.7	16.8	2.52	228	11.8	104	3.04	3.54	1.15	4.6	0.76	4.9	1.07
STV_LS_17	CL-5	0.16	14.7	146	1.41	0.71	3.04	0.3	6.8	16.4	2.57	225	12.1	102	2.93	3.58	1.18	4.23	0.75	4.95	1.04
STV_LS_45	CL-13	0.43	12.3	112	0.83	0.47	2.53	bdl	5.2	13.7	2.27	225	11.5	88	2.49	3.86	1.13	3.98	0.76	5.16	1.12
STV_LS_46	CL-14	0.32	8	84.1	0.57	0.37	2.32		3.8	10.4	1.75	229	9.1	68	2.06	3.19	1.05	3.58	0.63	4.39	0.98
STV_LS_47	CL-15	0.31	8.3	86.8	0.54	0.36	2.23	0.4	3.9	10.6	1.77	233	9.4	67	2.09	2.82	1.1	3.9	0.65	4.62	0.94
STV_LS_48	CL-16	0.19	10.2	110.5	1.06	0.52	2.64	0.2	5.4	14	2.04	248	10.6	78	2.34	3.08	1.03	3.68	0.58	4.16	0.87
STV_LS_18	Dome	0.52	14.9	128	1.17	0.58	3	0.5	5.7	14.6	2.29	226	11.2	89	2.9	3.35	1.13	4.46	0.77	4.8	1.09
STV_LS_21	YTF	0.1	4	91	0.23	0.18	1.08	bdl	2.6	6.8	1.23	460	6.8	40	1.46	2.41	0.91	2.96	0.56	3.37	0.77
STV_LS_22	YTF	0.13	7.5	78.5	0.65	0.34	2.5	0.2	5	13.4	2.07	218	10.6	87	2.67	3.25	1.1	3.93	0.64	4.49	0.95
STV_LS_24	YTF	0.1	9.6	96.9	0.7	0.41	2.34	0.4	4.8	12.6	2.01	216	9.9	83	2.32	2.99	1.08	3.84	0.67	4.31	0.91
STV_LS_25	YTF	0.13	6.9	77.6	0.56	0.35	1.94	0.3	4	10.2	1.57	250	8.5	63	1.82	2.6	0.89	3.11	0.54	3.58	0.77
STV_LS_26	YTF	0.08	4.1	90.9	0.24	0.15	1.12	0.1	2.6	7.3	1.27	459	6.7	40	1.32	2.47	0.8	2.91	0.54	3.53	0.74
STV_LS_27	YTF	0.21	9.5	96	0.81	0.45	2.87	0.3	5	12.2	1.94	257	8.8	72	2.15	2.71	0.96	3.14	0.54	3.34	0.74
2024 fieldwork																					
STV_LS_100	LL lava	0.52	13.9	129.5	1.28	0.66	2.92	0.2	6	14.7	2.02	221	10	90	2.34	2.76	0.93	3.77	0.59	4.05	0.89
STV_LS_102	LL lava	0.2	13.1	127	1.2	0.62	2.75	0.1	6.3	15	2.15	226	11	90	2.6	2.91	1.01	3.98	0.62	3.97	0.84
STV_LS_103	LL lava	0.16	13	122	1.16	0.59	2.61	0.1	6	14	2.11	222	9.8	89	2.43	2.93	0.99	3.71	0.63	4	0.83
STV_LS_104	LL lava	0.14	13.1	119.5	1.21	0.67	2.9	0.1	6.1	14	2.09	232	9.8	89	2.53	2.92	0.98	3.86	0.59	4.06	0.82
STV_LS_130	UL lava	0.53	14.6	127.5	1.26	0.6	2.58	0.1	6.4	14.4	2.11	229	10.8	90	2.56	2.82	1.01	3.82	0.63	4.11	0.86
STV_LS_131	UL lava	0.53	14.3	124	1.28	0.63	2.86	0.1	6.3	14.4	2.09	225	10.4	89	2.55	2.84	1.1	3.61	0.61	4.06	0.86
STV_LS_154	Roseau lava	0.27	13.8	148	1.27	0.69	3.01	0.1	6.6	15.9	2.21	209	11.8	99	2.97	3.03	1.1	4.56	0.75	4.64	1.04
STV_LS_160	Roseau lava	0.23	14.4	145.5	1.27	0.72	3.21	0.6	6.7	16.1	2.36	208	11	98	2.84	3.26	1.09	4.15	0.71	4.69	0.96
STV_LS_167	Roseau lava	0.12	9.1	105.5	0.7	0.39	2.28	0.1	5	13.1	1.99	229	9.8	82	2.38	3.04	1.15	3.95	0.71	4.29	0.94
STV_LS_106	LL dyke - core	0.43	16.3	133.5	1.19	0.62	2.55	0.1	6	14.9	2.29	214	11.5	100	2.85	3.18	1.04	4.36	0.7	4.49	0.99

Table 2 (continued)

STV_LS_107	LL dyke - edge	0.63	16	141.5	1.22	0.65	2.76	0.1	6.5	15.8	2.41	219	11.8	104	2.77	3.41	1.02	4.32	0.74	4.72	1.06
STV_LS_132	UL dyke	0.2	11.4	133.5	0.96	0.61	2.59	0.1	6.1	15.3	2.38	221	12.2	102	2.84	3.83	1.26	4.7	0.86	5.08	1.17
STV_LS_133	UL dyke	0.17	11.6	128	1.01	0.58	2.4	0.1	5.9	14.7	2.25	223	12.4	100	2.7	3.77	1.2	4.99	0.85	5.35	1.17
STV_LS_134	UL dyke	0.14	11.8	131.5	1.07	0.56	2.39	0.1	5.9	14.8	2.16	217	11	100	2.86	3.64	1.18	4.8	0.8	5.22	1.14
2020-2021 eruption																					
411-SVG-1*	U5 scoria	0.50	12.1	109.9	0.95	0.51	2.69	0.2	5.4	13.8	1.95	217	9.6	81	2.31	2.87	1.04	3.58	0.63	4.13	0.90
411-SVG-2*	U5 scoria	0.53	12.6	114.3	1.01	0.55	2.83	0.2	5.6	14.6	2.03	214	10.1	85	2.46	3.01	1.05	3.72	0.65	4.30	0.94
411-SVG-7*	U5 scoria	0.53	12.4	112.8	0.99	0.53	2.74	0.2	5.6	14.5	2.03	209	10.3	84	2.44	3.04	1.07	3.87	0.67	4.45	0.97
411-SVG-8*	U5 scoria	0.55	13.2	119.7	1.05	0.57	2.90	0.2	5.8	15.0	2.09	212	10.5	89	2.52	3.11	1.06	3.89	0.67	4.45	0.96
411-SVG-11a*	U5 scoria	0.58	13.1	119.7	1.06	0.57	2.95	0.2	5.9	15.3	2.14	213	10.7	89	2.53	3.19	1.06	3.98	0.69	4.55	1.00
411-SVG-11B*	U5 scoria	0.57	13.3	119.6	1.06	0.57	2.95	0.2	5.9	15.2	2.12	216	10.6	89	2.54	3.15	1.09	3.93	0.68	4.55	0.99
411-SVG-12A*	U5 scoria	0.58	13.5	119.7	1.19	0.59	2.93	0.2	6.0	15.3	2.14	210	10.6	88	2.54	3.18	1.09	3.96	0.69	4.59	0.99
411-SVG-12B-2*	U5 scoria	0.59	13.3	119.7	1.20	0.60	2.88	0.2	5.9	15.2	2.12	212	10.5	87	2.51	3.14	1.09	3.89	0.68	4.49	0.98
411-SVG-12B-2*	U5 scoria	0.59	13.3	120.5	1.21	0.60	2.91	0.2	5.9	15.3	2.13	211	10.6	88	2.54	3.16	1.10	3.92	0.68	4.55	0.99
Sample #	**Unit**	Er	Yb	Y	Lu	Tm	Sc	V	Cr	Ga	W	**Th/ Nb**	**La/ Sm**	**Ba/ Th**	**U/ Th**	**Ce/ Yb**	**Th/ Yb**	**Dy/ Yb**	**Ba/ La**	**Dy / Dy***	**Eu / Eu***
		ppm	ppm	ppm	ppm	ppm	ppm	ppm	ppm	ppm	ppm										
2023 fieldwork																					
STV_LS_3	CL-1	2.73	2.65	25.2	0.46	0.42	35.1	286	12	20	0.8	0.43	2.02	108	0.52	5.13	0.42	1.61	22.50	1.17	0.99
STV_LS_4a	CL-1	2.97	2.95	28.8	0.49	0.46	35.4	273	17	19.7	0.9	0.39	1.70	112	0.53	4.95	0.39	1.75	21.33	1.27	0.90
STV_LS_4b	CL-1	2.97	2.99	29.5	0.49	0.48	35.8	265	18	20	0.7	0.39	1.52	107	0.51	5.02	0.40	1.61	22.54	1.19	0.85
STV_LS_5a	CL-10	2.61	2.62	26.3	0.4	0.38	34.2	270	51	18.9	0.7	0.42	1.82	114	0.51	5.73	0.45	1.55	23.02	1.10	0.81
STV_LS_5b	CL-10	2.74	2.75	26.6	0.39	0.45	35.1	258	41	19.1	0.8	0.44	1.92	110	0.53	5.35	0.44	1.50	22.46	1.07	0.96
STV_LS_6	CL-7	2.71	2.6	26.1	0.41	0.4	35	277	48	19.1	2.5	0.38	1.69	108	0.54	5.54	0.46	1.60	22.86	1.14	0.94
STV_LS_7	CL-9*	2.17	1.9	20.7	0.32	0.34	46.8	307	409	17.1	0.7	0.50	1.89	86	0.41	6.00	0.57	1.86	20.76	1.27	1.00
STV_LS_8	CL-2	3.43	2.81	25.7	0.46	0.45	35.2	277	36	19.2	1.1	0.41	1.85	109	0.49	5.09	0.42	1.56	23.04	1.14	0.88
STV_LS_10	CL-2	2.63	2.65	25.6	0.44	0.43	34.5	277	32	18.8	0.7	0.40	1.78	111	0.50	5.25	0.43	1.71	22.50	1.23	0.90
STV_LS_11	CL-4	2.41	2.69	24.9	0.39	0.4	36.8	284	51	18.8	0.9	0.38	1.89	106	0.51	5.28	0.43	1.53	22.18	1.11	1.00
STV_LS_13	CL-9*	2.14	2.01	20.8	0.33	0.34	47.6	303	364	16.4	0.7	0.41	1.85	107	0.43	5.47	0.44	1.75	21.36	1.22	0.91
STV_LS_14	CL-11*	2.19	2.36	22.7	0.34	0.31	46.5	302	320	17.9	0.8	0.43	1.78	109	0.50	4.87	0.40	1.62	22.17	1.18	0.98
STV_LS_15	CL-12	2.67	2.92	26.7	0.43	0.43	30.8	219	9	19.1	0.8	0.34	1.72	135	0.60	4.66	0.31	1.57	23.37	1.18	0.89
STV_LS_16	CL-5	3.08	3.03	29.4	0.51	0.48	33.6	262	22	18.7	0.8	0.42	1.89	106	0.48	5.54	0.46	1.62	22.09	1.16	0.88
STV_LS_17	CL-5	2.96	3.07	30.2	0.49	0.47	34.1	260	21	18.8	0.7	0.46	1.90	104	0.50	5.34	0.46	1.61	21.47	1.16	0.93
STV_LS_45	CL-13	3.15	3.34	31.2	0.51	0.47	31.8	255	5	19.1	<0.5	0.33	1.35	135	0.57	4.10	0.25	1.54	21.54	1.21	0.89
STV_LS_46	CL-14	2.73	2.51	26.6	0.41	0.42	43.5	348	12	19.4	0.7	0.25	1.19	148	0.65	4.14	0.23	1.75	22.13	1.35	0.96
STV_LS_47	CL-15	2.66	2.74	26.3	0.41	0.44	40.7	350	11	19.7	0.7	0.24	1.38	161	0.67	3.87	0.20	1.69	22.26	1.33	1.02
STV_LS_48	CL-16	2.82	2.5	25.8	0.4	0.42	28.9	216	24	18.3	0.7	0.40	1.75	104	0.49	5.60	0.42	1.66	20.46	1.18	0.94
STV_LS_18	Dome	3	3.07	29.8	0.45	0.47	37.2	274	18	19.1	1	0.39	1.70	109	0.50	4.76	0.38	1.56	22.46	1.17	0.90
STV_LS_21	YTF	2.07	1.93	20.8	0.32	0.29	47.6	433	37	17.5	0.7	0.21	1.08	396	0.78	3.52	0.12	1.75	35.00	1.36	1.05
STV_LS_22	YTF	2.82	2.69	26.7	0.43	0.45	24.5	192	30	20.8	0.7	0.26	1.54	121	0.52	4.98	0.24	1.67	15.70	1.23	0.95

Table 2 (continued)

STV_LS_24	YTF	2.71	2.64	25.8	0.45	0.4	30.6	240	40	19.2	0.8	0.30	1.61	138	0.59	4.77	0.27	1.63	20.19	1.21	0.98
STV_LS_25	YTF	2.28	2.07	22	0.32	0.35	35.1	292	43	19	0.6	0.29	1.54	139	0.63	4.93	0.27	1.73	19.40	1.24	0.96
STV_LS_26	YTF	2.1	1.88	20.5	0.32	0.34	49.5	448	44	17	0.7	0.21	1.05	379	0.63	3.88	0.13	1.88	34.96	1.45	0.92
STV_LS_27	YTF	2.16	1.92	21.2	0.3	0.31	31.5	259	133	19.3	0.8	0.28	1.85	119	0.56	6.35	0.42	1.74	19.20	1.16	1.01
2024 fieldwork																					
STV_LS_100	LL lava	2.74	2.66	23.6	0.4	0.35	34.9	274	128	21.5	0.9	0.44	2.17	101	0.52	5.53	0.48	1.52	21.58	1.08	0.89
STV_LS_102	LL lava	2.59	2.49	23.4	0.37	0.37	35.7	268	137	20.5	0.5	0.44	2.16	106	0.52	6.02	0.48	1.59	20.16	1.09	0.91
STV_LS_103	LL lava	2.57	2.67	22.9	0.37	0.4	33.6	259	134	21.4	0.9	0.44	2.05	105	0.51	5.24	0.43	1.50	20.33	1.06	0.92
STV_LS_104	LL lava	2.57	2.52	23.8	0.37	0.4	36.1	270	136	20.3	0.6	0.42	2.09	99	0.55	5.56	0.48	1.61	19.59	1.12	0.90
STV_LS_130	UL lava	2.51	2.48	24.4	0.39	0.37	36	263	116	20.8	0.5	0.49	2.27	101	0.48	5.81	0.51	1.66	19.92	1.13	0.95
STV_LS_131	UL lava	2.52	2.57	23.8	0.37	0.38	34.1	256	117	20.8	0.6	0.45	2.22	97	0.49	5.60	0.50	1.58	19.68	1.09	1.06
STV_LS_154	Roseau lava	3.19	3.17	28.2	0.43	0.51	37	247	49	21.8	< 0.5	0.42	2.18	117	0.54	5.02	0.40	1.46	22.42	1.07	0.91
STV_LS_160	Roseau lava	3.03	2.68	27.8	0.45	0.48	37.1	248	58	21.5	0.6	0.40	2.06	115	0.57	6.01	0.47	1.75	21.72	1.21	0.91
STV_LS_167	Roseau lava	2.8	2.83	26.3	0.5	0.42	36.1	286	17	23.1	0.6	0.31	1.64	151	0.56	4.63	0.25	1.52	21.10	1.14	1.02
STV_LS_106	LL dyke - core	2.94	3.15	27.7	0.48	0.46	33.1	250	20	22	0.5	0.47	1.89	112	0.52	4.73	0.38	1.43	22.25	1.06	0.86
STV_LS_107	LL dyke - edge	3.06	2.84	28.5	0.45	0.49	34.8	257	18	21.7	0.5	0.44	1.91	116	0.53	5.56	0.43	1.66	21.77	1.18	0.82
STV_LS_132	UL dyke	3.58	3.36	32.1	0.54	0.55	33.5	243	8	23.3	0.7	0.37	1.59	139	0.64	4.55	0.29	1.51	21.89	1.14	0.91
STV_LS_133	UL dyke	3.31	3.49	32.2	0.49	0.5	35.5	245	7	22.8	<0.5	0.42	1.56	127	0.57	4.21	0.29	1.53	21.69	1.18	0.85
STV_LS_134	UL dyke	3.52	3.39	30.2	0.57	0.57	31.7	223	8	21.9	0.6	0.45	1.62	123	0.52	4.37	0.32	1.54	22.29	1.18	0.87
2020–2021 eruption																					
411-SVG-1**	U5 scoria	2.56	2.60	24.7	0.41	0.39	29.8	233	26	17.9		0.35	1.87	116	0.54	5.30	0.36	1.59	20.49	1.14	0.99
411-SVG-2**	U5 scoria	2.69	2.73	26.0	0.43	0.41	29.3	227	23	17.9		0.36	1.88	113	0.54	5.35	0.37	1.58	20.26	1.14	0.96
411-SVG-7**	U5 scoria	2.75	2.83	26.1	0.44	0.42	33.5	236	20	18.3		0.36	1.85	114	0.54	5.12	0.35	1.57	20.00	1.15	0.96
411-SVG-8**	U5 scoria	2.77	2.77	26.9	0.44	0.42	29.0	237	21	17.9		0.36	1.87	114	0.54	5.43	0.38	1.61	20.62	1.16	0.94
411-SVG-11a**	U5 scoria	2.82	2.87	27.0	0.45	0.44	29.7	246	22	18.1		0.36	1.86	113	0.54	5.34	0.37	1.58	20.18	1.15	0.92
411-SVG-11B**	U5 scoria	2.81	2.88	27.2	0.45	0.43	30.3	254	22	18.5		0.36	1.86	112	0.53	5.26	0.37	1.58	20.38	1.15	0.95
411-SVG-12A**	U5 scoria	2.83	2.90	27.0	0.45	0.44	31.0	258	25	18.2		0.41	1.88	100	0.50	5.28	0.41	1.58	20.09	1.15	0.94
411-SVG-12B-2**	U5 scoria	2.80	2.88	26.8	0.45	0.42	31.1	256	25	17.9		0.42	1.87	100	0.50	5.26	0.41	1.56	20.40	1.13	0.96
411-SVG-12B-2**	U5 scoria	2.81	2.85	27.2	0.45	0.43	30.8	259	25	18.2		0.41	1.87	100	0.50	5.37	0.42	1.59	20.40	1.15	0.96

bdl – below detection limit.

* Mafic Crater Lava.

** Data from Holli Frey analysed via dissolution on an Agilent 8900 ICP-MS at the Department of Geosciences, Union College, New York.

No data for STV_LS_20 due to contamination.

Table 3 New $^{40}Ar/^{39}Ar$ data for La Soufrière

Sample #	Location	$^{40}Ar/^{36}Ar_i \pm 2$ s		Isochron		Plateau		*N*	^{39}Ar %	MSWD
				Age (ka) ± 2 s		Age (ka) ± 2 s				
STV-LS-6	Crater	296.5	± 3.7	16.4	± 19.8	5.7	± 4.4	11/16	90.5	0.92
STV-LS-46	Crater	298.2	± 1.3	12.3	± 18.9	7.9	± 7.7	13/14	98.3	0.46
STV-LS-5a	Crater	299.2	± 1.7	21.6	± 11.0	25.2	± 3.8	16/17	99.7	0.59
STV-LS-103	Lower Larikai	298.4	± 2.2	5.4	± 13.7	4.4	± 4.2	12/18	91.4	0.56
STV-LS-100	Lower Larikai	299.3	± 0.9	22.6	± 15.5	33.7	± 8.0	15/18	95.5	0.36
STV-LS-167	Roseau	298.5	± 2.3	14.7	± 7.9	14.5	± 3.1	14/18	95.0	1.03
STV-LS-154	Roseau	298.5	± 1.3	31.9	± 8.9	31.5	± 4.0	15/19	90.7	1.01
VSG-2	Jacobs well	298.6	± 0.5	474.0	± 37.6	475.6	± 28.3	13/14	99.8	0.55

Ages calculated relative to 1.1864-Ma Alder Creek sanidine standard (Jicha et al. 2016) using the decay constants of Min et al. (2000)

Atmospheric $^{40}Ar/^{36}Ar = 298.56 \pm 0.31$ (Lee et al. 2006)

N, number of incremental heating steps

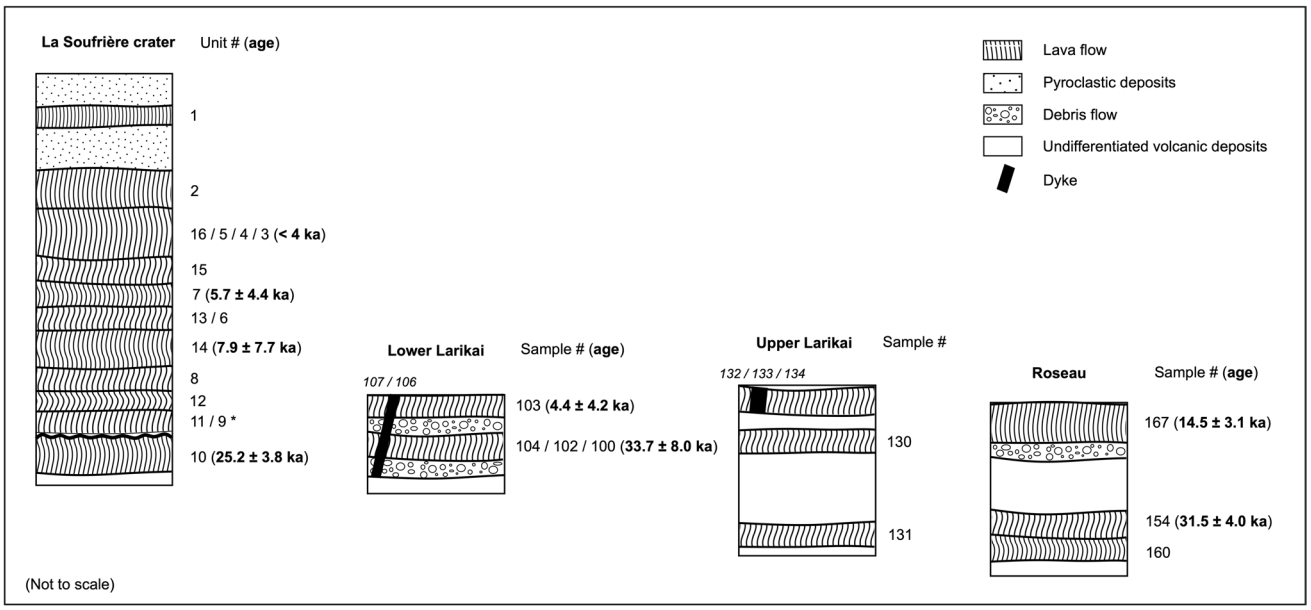

Fig. 4 Stratigraphic logs (not to scale) for the current La Soufrière crater, lower Larikai, upper Larikai and Roseau valley for samples collected. Samples shown in relative age order with known ages labelled (bold). Unit number used for the crater stratigraphic log and sample number (e.g. STV_LS_100) for all other locations. Asterix indicates Mafic Crater Lava unit (~8 wt.% MgO). Dyke sample numbers in italic. Observed pyroclastic and debris flow units shown. Blank spaces in the logs indicate absence of exposure

preferentially uptakes HREE, and amphibole or clinopyroxene fractionation that prefer MREE. Dy/Dy* values for the La Soufrière lavas are positively correlated with Dy/Yb and support amphibole or clinopyroxene fractionation (Davidson et al. 2013) consistent with the subtle spoon-shaped patterns of MREE in Fig. 7. The negative relationship between Dy/Dy* and incompatible La (Fig. 8b) strongly suggests that evolved magmas experienced more amphibole or clinopyroxene fractionation. Amphibole fractionation is consistent with the abundance of amphibole (and plagioclase) rich cumulates (Tollan et al. 2012) and water-rich magmas (Cooper et al. 2020) at St. Vincent.

$^{40}Ar/^{39}Ar$ ages

New $^{40}Ar/^{39}Ar$ ages for seven lava samples and a xenolith from La Soufrière are reported in Table 3 and their stratigraphic context shown schematically in Fig. 4 (unsuccessful age determinations reported in the Appendix). $^{40}Ar/^{39}Ar$ age spectra, inverse isochron plots and the full $^{40}Ar/^{39}Ar$ dataset for all samples are reported in the Supplementary Materials.

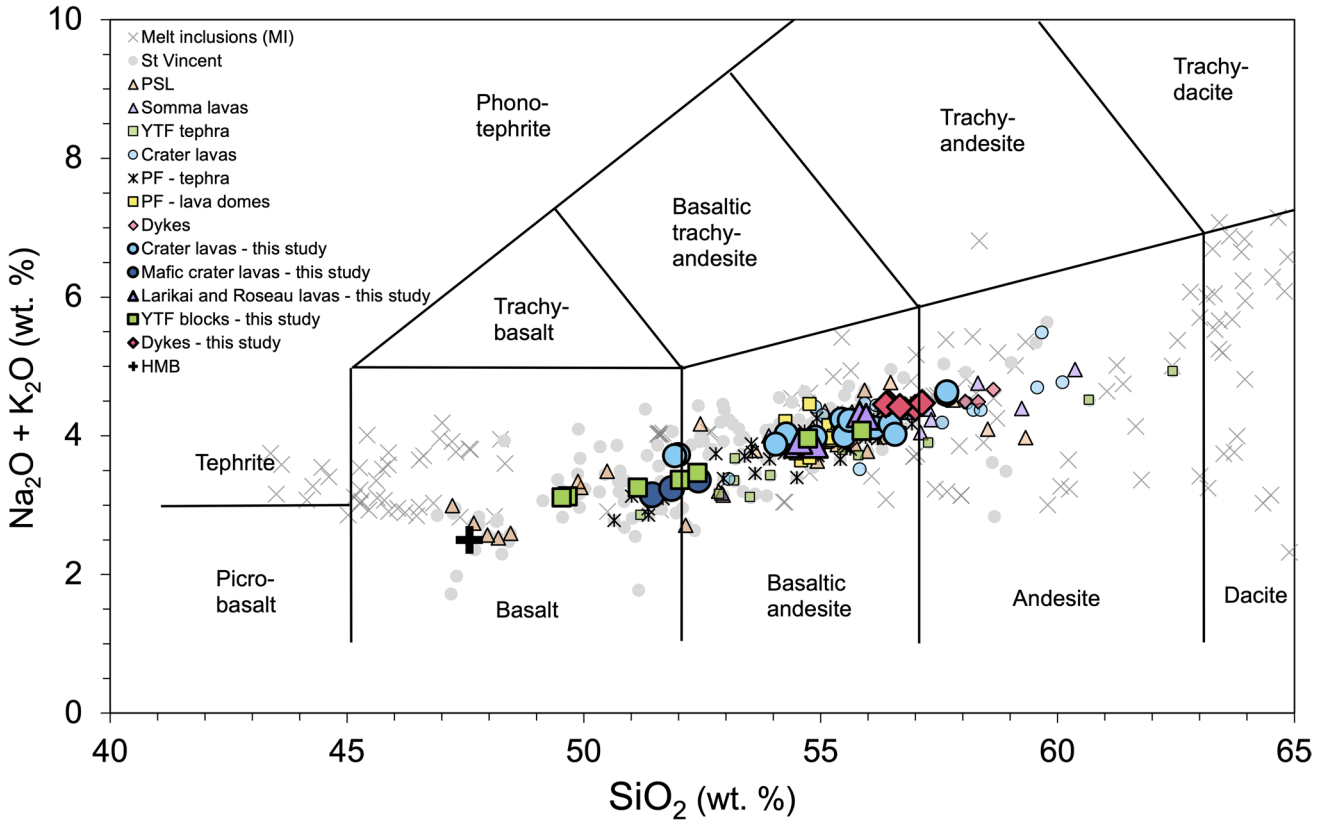

Fig. 5 Total alkali versus silica (TAS) diagram after Le Bas et al. (1986). PSL, pre-Somma lavas; CL, Crater Lavas; YTF, Yellow Tuff Formation; PF, Pyroclastic Formation. New data for samples analysed in this study are shown as large bold symbols with thick outlines; previous data for La Soufrière eruption products are shown as smaller faded symbols (Rowley 1978; Heath et al. 1998; Cole et al. 2019). Previous data for lavas and melt inclusions (MI) from older volcanic centres on St. Vincent are shown as grey circles and crosses (data from Robertson 2002 and GEOROC: Lacroix 1949; Bardintzeff et al., 1983, 1984; Graham and Thirlwall 1981; Dostal et al. 1983; Thirlwall et al. 1994; Heath et al. 1998; Plank 2005; Bouvier et al. 2008; Cole et al. 2019; Fedele et al. 2021). A high-magnesium basalt (HMB; RSV49; Robertson 2002) is shown to illustrate a likely parent to La Soufrière magmas (Melekhova et al. 2015)

Dates agree, within uncertainty, with estimated stratigraphic positions from field observations. Three of four crater lavas were successfully dated. Crater lava STV_LS_46 (Unit 14) in the southeastern crater wall is dated at 7.9 ± 7.7 ka, and STV_LS_6 (Unit 7) in the eastern crater wall is 5.7 ± 4.4 ka (Fig. 2a). The high uncertainty associated with these young dates, due to low abundances of K_2O (Fig. 6e) and hence radiogenic Ar, means determining the exact emplacement chronology and drawing conclusions about the morphology of the crater is not possible, but it does confirm their young age relative to other lavas from La Soufrière. The lowermost crater lava unit sampled (STV_LS_5a) is dated at 25.2 ± 3.8 ka and sits at the relative base of the new outer crater in the northern wall (Unit 10; Fig. 2a). This unit correlates to the 'pre-historic coulee' identified by Sigurdsson (1981). It also immediately underlies the Mafic Crater Lava of Units 9 and 11, which are shown in Sigurdsson's 1981 map to extend to the 'coulee flow front'. Although we do not have ages for these lavas, Unit 7 (dated at 5.7 ± 4.4 ka) lies immediately above the northern extent of Unit 9 without clear stratigraphic break (Sigurdsson 1981; scree covers base of Unit 7 in Fig. 2). We therefore propose that there is a significant unconformity between Units 10 and 7 corresponding to almost 20 kyr. Previously, the crater lavas had been estimated at ~ 4 ka by association with the YTF eruption (Rowley 1978; Heath 1997; Robertson 2002); however, our new ages show that the lowermost crater lavas are significantly older than the upper crater lavas, consistent with the geological map of Sigurdsson (1981) who places some crater lavas within or beneath the pre-YTF debris flow deposits. Evidently, there was either a sustained hiatus in volcanic activity within the crater or Unit 10 (and other lower crater lavas) originate from an earlier phase of volcanism (e.g. Somma). We discuss these two possibilities in a later section.

New dates for the lavas in Larikai valley range from 33.7 ± 8.0 to 4.4 ± 4.2 ka and in Roseau valley from 31.5 ± 4.0 to 14.5 ± 3.1 ka (Fig. 4). These dates are considerably younger than previously dated pre-Somma lavas on the eastern flanks (Table 4) but overlap with a low-precision age of a lava from the southeastern flanks that could

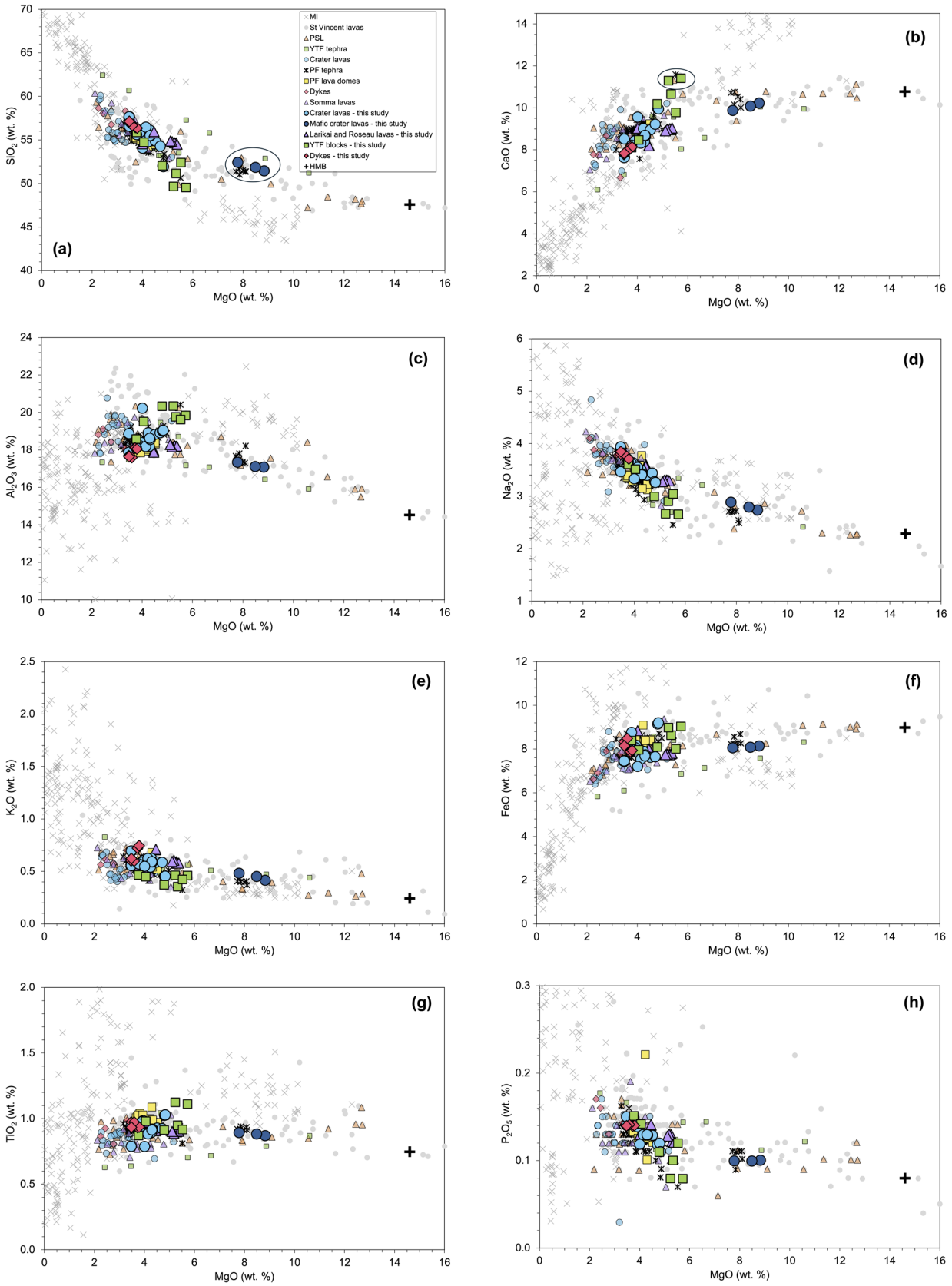

Fig. 6 Major oxides versus MgO (wt.%). **a** SiO_2. **b** CaO. **c** Al_2O_3. **d** Na_2O. **e** K_2O. **f** FeO(T). **g** TiO_2. **h** P_2O_5. Mafic Crater Lava unit (STV_LS_7, 13 and 14) circled in **a**. High-Ca YTF lava blocks (STV_LS_21 and 26) circled in **b**. Symbology and abbreviations as in Fig. 5

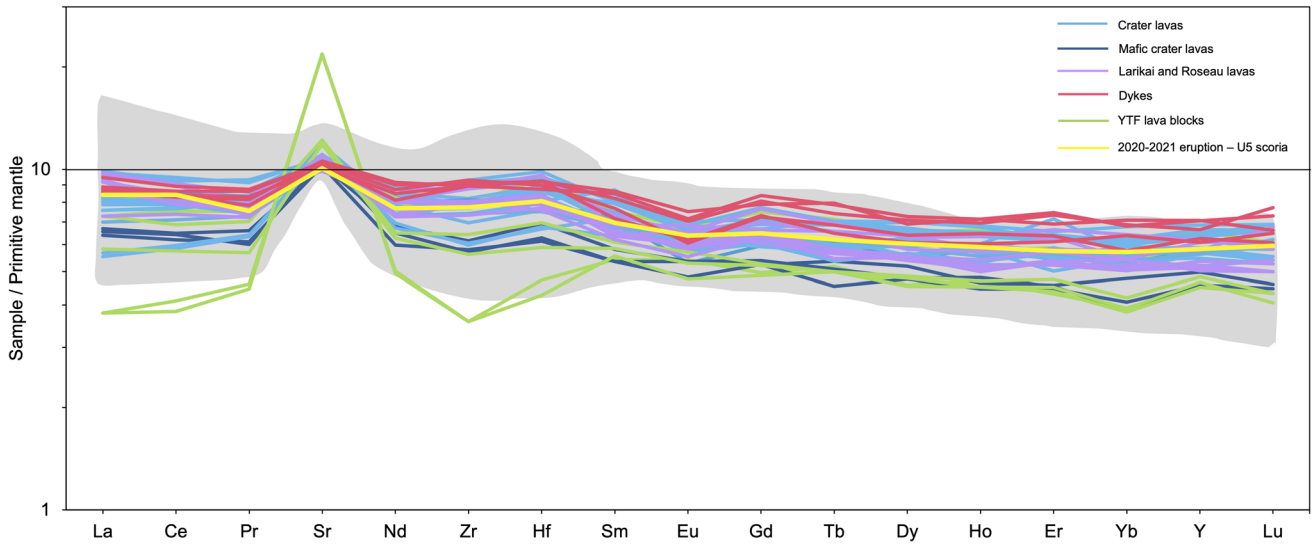

Fig. 7 Spider diagram for REE elements plus Sr, Zr and Hf normalised to the primitive mantle (Sun and McDonough 1989). Colours as in Fig. 5. Grey shading shows previous St. Vincent lava and tephra data (GEOROC: Graham and Thirlwall 1981; Dostal et al. 1983; Bardintzeff et al., 1984; Thirlwall, 1994; Heath et al. 1998; Plank 2005; Cole et al. 2019). U5 scoria from 2020/2021 eruption at La Soufrière from Holli Frey; average shown as all data are near-identical (see Table 2)

have originated from either Morne Garu or La Soufrière (11 ± 14 ka, Table 4; Heath 1997; Robertson 2005). The youngest lower Larikai lava (4.4 ± 4.2 ka; STV_LS_103) corresponds in age to the younger crater lavas with which it likely correlates. This lava is crosscut by a dyke (Figs. 3d, 4), meaning effusive activity continued on the western flank after 4 ka, possibly related to the eruption of the very youngest crater lavas or the Pyroclastic Formation. Interestingly, the young lower Larikai dyke is geochemically very similar to the youngest crater lava (Unit 1) that appears to be dyke fed (Fig. 2b).

The hornblende-gabbro xenolith sample (VSG-2; amph + plag + ol) gave a considerably older age of 475.6 ± 28.3 ka, corresponding to much earlier, pre-Somma (0.18 to 0.69 Ma) magmatism. This date records when the xenolith ceased exchanging argon with the atmosphere, perhaps due to cooling and/or lack of melt present, but not its original formation. Despite its older age, the xenolith was entrained and brought to the surface by a younger (albeit unidentified) La Soufrière magma, indicating that these magmas were sourced from regions at similar or greater depth than those of the pre-Somma magmatic period.

Discussion

Stratigraphic sequence

In Fig. 9a, all dated eruption products from La Soufrière are arranged in stratigraphic order using radiocarbon, marine fossil, K-Ar and $^{40}Ar/^{39}Ar$ dates, as well as observed stratigraphic positions to assess chemical variation over time and the presence of any hiatuses that could record perturbations to the magmatic system or the volcanic edifice. For published ages, we have used the author's original lithological and stratigraphic designation. We have used a logarithmic time scale to enable the entire history of the volcano to be captured in a single figure.

Given the relative completeness of the stratigraphic and radiometric catalogue in Fig. 9a, it is reasonable to assume that where there are gaps of few or no dates, these may correspond to hiatuses in the eruption record. Two prominent gaps are observed. The first is between 33.7 ± 80 and 180 ± 21 ka and the second between ~ 4 and 11 ka. Although the first gap was apparent from literature data prior to our study, new $^{40}Ar/^{39}Ar$ ages from the oldest Roseau and lower Larikai lavas narrow the gap and provide an upper age constraint for the Somma stage. This gap brackets the postulated age for the Baleine collapse (~ 50 ka; Le Friant et al. 2009), suggesting that either this event removed part of the stratigraphic record or occurred during a period of volcanic quiescence.

The second less pronounced gap, between ~ 4 and 11 ka, corresponds to the previously poorly dated Somma collapse that separates the Somma stage from subsequent building and cratering of the La Soufrière edifice (YTF, Crater Lavas and Pyroclastic Formation stages; Fig. 9a). Several lines of evidence define this gap. Firstly, there is a break in the marine tephra record between 3 and 15 ka (Table 4), with the younger tephra plausibly corresponding to the YTF. On

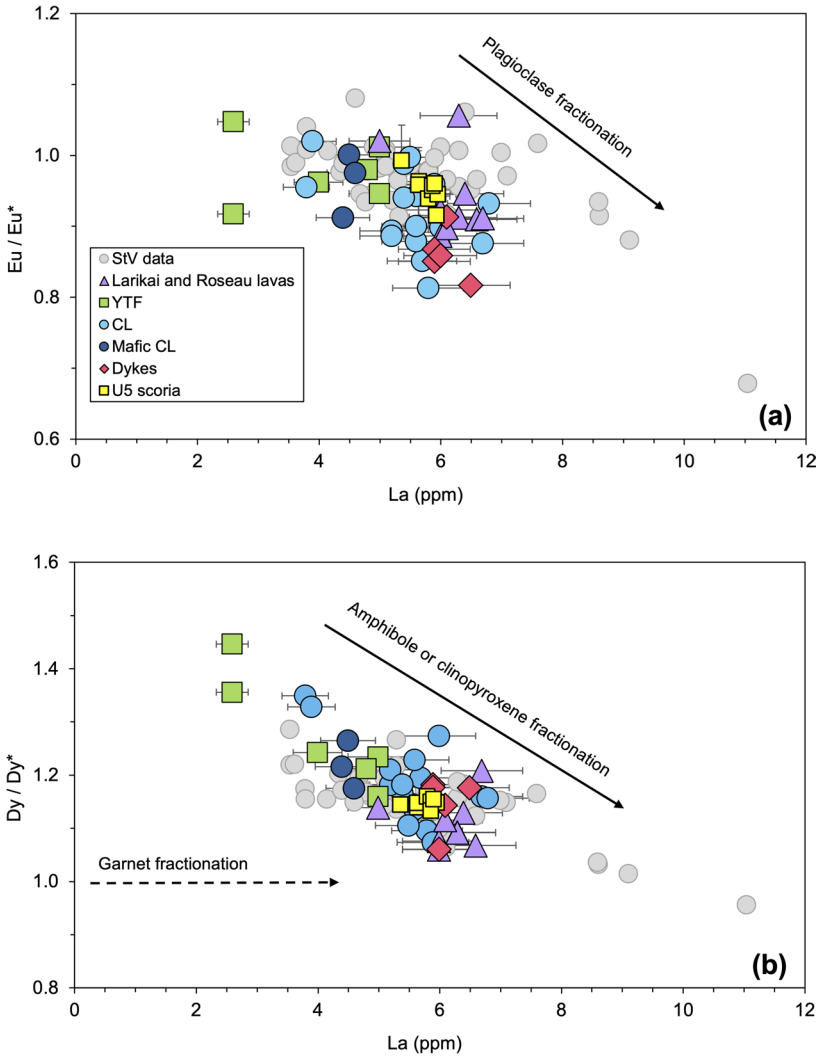

Fig. 8 Plots of REE ratios versus La, as an index of differentiation. **a** Eu/Eu* to determine the degree of plagioclase fractionation and **b** Dy/Dy* to determine the degree of clinopyroxene or amphibole fractionation experienced by magmas. Eu/Eu* calculated as interpolation between Sm and Gd (see text; Tang et al. 2021) and normalised to chondritic values of Nakamura (1974). Dy/Dy* calculated after Davidson et al. (2013)

land, our new data reveal a marked unconformity within the crater lava sequence between 25 ka (Unit 10 of Fig. 2a) and the overlying upper crater lavas at ≤ 8 ka. A single lava flow from Roseau valley (STV_LS_167) was emplaced during this time at 14.5 ± 3.1 ka, perhaps placing a tighter lower bound on the unconformity as the youngest lava dated in the proposed Somma stage (see below). Unfortunately, the large uncertainties associated with our young $^{40}Ar/^{39}Ar$ ages in the crater (5.7 ± 4.4 ka and 7.9 ± 7.7 ka; Units 7 and 14) and lower Larikai valley (4.4 ± 4.2 ka), arising due to their low K_2O content, preclude a tight upper constraint on the proposed Somma collapse gap in Fig. 9a. Furthermore, on radiometric grounds alone, it is not possible to establish whether these young crater lavas pre-date or post-date the YTF (known to overlie the Somma collapse debris flows; Sigurdsson 1981). The geological map of Sigurdsson (1981) indicates that most Crater Lavas overlie the Brown Tuff in the south crater wall and cross-cut it in the northwest crater wall. If the Brown Tuff is contemporaneous with the YTF, as suggested by Sigurdsson, then the young crater lavas are younger than the YTF (as shown in Fig. 9a). It is not clear how many individual eruptions the YTF represents. Rowley (1978) and Hay (1959) present radiocarbon dates of pyroclastic flows that *overlie* YTF air-fall deposits at 4325 ± 95, 4090 ± 50 and 3890 ± 300 years BP, placing a minimum age constraint on the YTF. Based on field relations and dates established in previous work (Sigurdsson 1981; Rowley 1978; Heath 1997) and in this study, we suggest that the age of the YTF lies between the oldest overlying pyroclastic material (brown diamonds in Fig. 9a; 4325 ± 95 years) and the oldest permissible age of the youngest Somma lava (14.5 ± 3.1 ka). The age of the YTF therefore overlaps with the proposed Somma collapse gap between approximately 4 and 11 ka on Fig. 9a. Eruption of the YTF would likely correspond to the end of the Somma collapse episode.

There is also geochemical evidence in support of the postulated Somma collapse gap; the oldest crater lavas (Units 9 and 11) are notably more mafic than lava above or below

stratigraphically (Fig. 9b) suggesting that a major perturbation to the sub-volcanic system occurred prior to their eruption. Collapse of the edifice and consequent decompression of the underlying system is one such process. Similarly, the YTF contains a number of lava blocks of distinct composition (Figs. 5 and 6), again consistent with perturbation of the magmatic system. Composition variability following the Mafic Crater Lava and the YTF decreases significantly (Fig. 9b).

Volcanic evolution

Our revised stratigraphy delineates the five key stages in the evolution of La Soufrière volcano: pre-Somma, Somma, Yellow Tuff Formation, Crater Lavas and Pyroclastic Formation (including historic lavas). These are described sequentially below with reference to new age constraints and compositional features. Our proposed volcanic evolution is shown schematically in Fig. 10.

Pre-Somma stage

The pre-Somma lavas represent the earliest and compositionally most diverse magmas at La Soufrière that now form the base of the volcanic edifice. Pre-Somma magmatism is dated at 690 to 180 ka, followed by a gap in the eruptive history from 180 to 34 ka (Table 4). The Baleine collapse, which is responsible for the prominent scarp north of the current crater (Fig. 1b), is estimated at 50 ka from offshore debris avalanche deposits and sedimentation rates (Le Friant et al. 2009). This event marks the end of the pre-Somma stage. We cannot discount the possibility that the Baleine collapse removed some of the intervening volcanic record, with the collapse removing much of the main volcanic edifice, allowing the Somma edifice to begin growing. The age of the Baleine collapse is not constrained by our new radiometric data but must pre-date the 33.7 ± 8.0 ka lava that outcrops in the lower Larikai valley.

Compositionally, the pre-Somma lavas cluster at basaltic andesite (Fig. 9b) but extend to high-magnesium basalts and show similar chemical variations to earlier volcanic centres on St. Vincent. Overall, the pre-Somma stage resembles magmatism elsewhere on St. Vincent in terms of compositional diversity (Fig. 9b).

Somma stage

The Somma edifice grew over a period of up to 46 kyr following the Baleine collapse and was itself terminated by the Somma collapse. Le Friant et al. (2009) previously suggested the Somma collapse occurred 'a few thousand years ago' based on average eruption rates and volumes; however, the $^{40}Ar/^{39}Ar$ ages and stratigraphic observations presented in this study provide new insight. A 33.7 ± 8.0 ka lava from lower Larikai and a 31.5 ± 4.0 lava from Roseau are the oldest dated samples that post-date the Baleine collapse and therefore could represent some of the earliest erupted magmas of the Somma stage. The lowermost crater lava collected in this study (Unit 10; Fig. 2a) is dated at ~ 25 ka, considerably older than previous estimates for the Crater Lavas (~ 4 ka; Heath 1997) and new ages for the upper crater lavas (≤ 8 ka) emplaced ≤ 30 m above (Fig. 3b), highlighting a major unconformity in the crater. The 25-ka lower crater lava could represent part of the Somma crater that survived the collapse and was covered by younger lavas, a slumped Somma lava block, or evidence a hiatus in the crater lava sequence. The 25-ka crater lava is similar in major and trace element geochemistry to many La Soufrière lavas, including the previously sampled Somma lavas and the younger upper crater lavas (Fig. 6), meaning geochemistry alone cannot be used to distinguish the origin of the lower crater lavas. Sigurdsson's (1981) field observations identified crater lavas within and below debris flow deposits from the Somma collapse in the southern crater wall that immediately underlie the Brown Tuff (YTF equivalent). The 25-ka crater lava may be a correlative of these lower crater lavas and is proposed as a vestige of the Somma stage of edifice construction. We tentatively attribute a 14.5 ± 3.1-ka lava (STV_LS_167) in the Roseau valley to this same stage, constraining the timing of the Somma collapse to younger than ~ 14 ka. This lava overlies a thick debris flow deposit (Figs. 3g, 4) that cannot easily be attributed to any particular collapse event.

Collapse of the Somma edifice must precede the younger crater lavas as they fill the depression created by the collapse of the edifice to the south. The Somma collapse would have blocked the existing vent, causing magmas to find a new route to the surface, as is common at volcanoes that experience repetitive edifice or flank collapse (e.g. Martinique, Tenerife, El Hierro; Maccaferri et al. 2017), resulting in a new vent location for the current La Soufrière edifice. Chemically, the Somma stage is more restricted than the pre-Somma stage with only basaltic andesites and rare low-magnesium basalts erupted.

Yellow Tuff Formation

The collapse of the Somma crater has previously been tentatively linked to the YTF eruption due to YTF deposits immediately overlying Somma collapse debris flow deposits, with no evidence of erosion (Rowley 1978; Sigurdsson 1981). Additionally, such a large collapse, illustrated by the tall remnant Somma collapse scar (Fig. 1c) wall and inferred volume of material removed, would have likely resulted in considerable depressurisation of the system and triggered a large explosive eruption (Manconi et al. 2009; Cassidy et al. 2018) supported by the thick and widespread YTF

eruption deposits (Rowley 1978), with lithic-rich layers containing lava blocks ≥ 70 cm (Fig. 3c). Two pyroclastic flows (likely YTF) that *underlie* and *overlie* a YTF air-fall deposit are radiocarbon dated and constrain the age of the fallout eruption to between 4.3 and 3.6 ka, similar to other dated YTF pyroclastic flow deposits (Rowley 1978). These dates coincide with the onset of the extrusion of the upper crater lavas (Fig. 9a) suggesting that the YTF immediately followed the Somma collapse and preceded the eruption of the younger crater lavas. YTF deposits are chemically diverse, ranging from low-magnesium basalts to basaltic andesites to andesites (Fig. 5; Heath et al. 1998). We suggest that the YTF can be viewed either as a transitional stage preceding the Crater Lavas or the climactic expression of the Somma stage. In either case, the YTF marks the last significant destabilisation of the magmatic system beneath La Soufrière.

Crater Lava stage

Following the Somma collapse and YTF eruption, a sustained period of edifice building is recorded by the sequence of lavas exposed in the crater with no observed intercalated pyroclastic material. New $^{40}Ar/^{39}Ar$ ages for two crater lavas (5.9 ± 4.4 and 7.9 ± 7.7 ka) and one of the youngest crater lavas (≤ 4 ka) without any detectable radiogenic Ar agree with previous estimates that the crater lavas are young and overlap in age with the YTF eruption (≤ 4.3 ka; Rowley 1978; Sigurdsson 1981; Heath 1997). Although previous eruptive histories propose volcanic activity during the emplacement of the Crater Lavas was constrained to the crater, the young lava flow in Larikai valley (4.4 ± 4.2 ka) and major destruction caused by the collapse of the Somma edifice suggest otherwise. Flank eruptions to the west of La Soufrière would have been facilitated by the southwestern Somma collapse reducing topography. Previous mapping in the La Soufrière crater also identified truncated lava flows and infilling of older smaller summit vents (Rowley 1978), suggesting explosive eruptions have continued to play a significant role in controlling the morphology of the crater. The young Larikai lava flow sits on top of a debris flow and is crosscut by a basaltic andesite dyke (Fig. 3d), implying volcanism on the western flank of La Soufrière was still occurring until much more recently than previously thought. The dyke could be related to the youngest crater lavas due to its compositional similarity to Unit 1, rather than the subsequent Pyroclastic Formation, which is often less evolved in composition.

We propose that the Crater Lava stage refers to the period of extrusive volcanism that post-dates the YTF and the observed unconformity between Units 10 and 7 in the northern crater wall. Compositionally, the Crater Lavas are predominantly basaltic andesites. However, two distinctive low-MgO basaltic units, together comprising the Mafic Crater Lava, are found at the base of the crater wall sequence. Published data indicate that some YTF tephra have similar MgO contents (Heath et al. 1998; Fig. 6), again suggesting some overlap between the YTF and Crater Lavas in terms of magma source regions perhaps driven by the Somma collapse.

Pyroclastic Formation and historic lavas

The Pyroclastic Formation, which post-dates both the Crater Lavas and the YTF, is comprised of alternating explosive and effusive eruptions. Pyroclastic Formation magmas are exclusively basaltic andesites with extremely limited compositional variation over the last ~ 4 ka, with the single exception of a mafic tephra of the 1902/1903 eruption (Fig. 9b). Historical eruptions mostly encompassed both effusive and explosive volcanism, with effusive volcanism often involving the extrusion of relatively small viscous lava domes that were confined to the crater. Extensive lava flows, as observed during the Somma and possibly Crater Lava stages, are not identified during the Pyroclastic Formation suggesting a difference in volume of material available, magma ascent rate or viscosity (Cassidy et al. 2018). The explosive eruptions during the Pyroclastic Formation phase are likely responsible for forming the general crater morphology observed today and carving out the vent that magmas erupt from.

Compositional evolution

In this section, we discuss the chemical evolution of La Soufrière, with cross references to other Lesser Antilles volcanic systems. Figure 9b shows compositional variation over the same stratigraphic sequence as Fig. 9a, highlighting the chemical uniformity of the La Soufrière magmatic system from ~ 34 ka onwards (lilac triangles upwards), with rare low-magnesium (6–10 wt.% MgO) basalts erupted during the YTF, the early Crater Lava period and in 1902/1903. Note that the marine tephra are glasses rather than whole-rocks, so are not representative of bulk magma chemistry. With the exception of the early Mafic Crater Lava, no sequential geochemical trends are observed in the Crater Lavas and the limited variation in major and trace element compositions (Figs. 5, 6, 7, 8) attests to a long-lived, homogenous period of volcanism with magmas tapping into a chemically buffered source region (Blundy 2022). Trace element ratios (e.g. Th/Nb, La/Sm, Th/Yb; Table 2) also attest to low sediment input and little crustal contamination (Hawksworth et al., 1991, Plank and Langmuir 1993; Elliot, 2003; Atlas et al. 2022), as do $^{87}Sr/^{86}Sr$ ratios that remain similar to the mantle (0.7040; Pushkar et al. 1973).

Table 4 Compiled K/Ar, $^{40}Ar/^{39}Ar$, ^{14}C and foraminifera dates for St. Vincent lavas, pyroclastic deposits and marine tephra in age order

Volcanic centre	Location	Sample #	Reference	Method	Age (yrs BP)
Pyroclastics					
La Soufrière 1902	Dry Wallibou	C45	Cole et al. 2019	^{14}C	20 ± 30
La Soufrière	Rabacca River	SVE-104	Heath 1997	^{14}C	20 ± 45
La Soufrière	Dry Wallibou River	SRR-3972	Robertson 1992	^{14}C	20 ± 4
La Soufrière	Rabacca River	SVE-102	Heath 1997	^{14}C	30 ± 45
La Soufrière	Dry Wallibou River	STV-123	Heath 1997	^{14}C	40 ± 45
La Soufrière	Dry Wallibou River	SRR-3973	Robertson 1992	^{14}C	45 ± 40
La Soufrière	Wallibou River	SVE-094	Heath 1997	^{14}C	55 ± 50
La Soufrière	Camariabou River	SVE-111	Heath 1997	^{14}C	70 ± 45
La Soufrière	Rabacca River	SVE-105	Heath 1997	^{14}C	75 ± 45
La Soufrière	Dry Wallibou River	SVE-090	Heath 1997	^{14}C	75 ± 40
La Soufrière	Sandy Bay	STV-112	Heath 1997	^{14}C	75 ± 45
La Soufrière 1812	Dry Wallibou	C4	Cole et al. 2019	^{14}C	79 ± 37
La Soufrière	Dry Wallibou River	SRR-3974	Robertson 1992	^{14}C	80 ± 40
La Soufrière 1812/1718	Wallibou coast	C49	Cole et al. 2019	^{14}C	90 ± 30
La Soufrière	Rabacca River	SVE-101	Heath 1997	^{14}C	90 ± 45
La Soufrière	Rabacca River	SVE-103	Heath 1997	^{14}C	100 ± 45
La Soufrière	Rabacca River	SVE-106	Heath 1997	^{14}C	105 ± 45
La Soufrière	Wallibou River	SVE-086	Heath 1997	^{14}C	120 ± 40
La Soufrière	Dry Wallibou River	SVE-097	Heath 1997	^{14}C	125 ± 45
La Soufrière	Wallibou River	SVE-085	Heath 1997	^{14}C	130 ± 45
La Soufrière	Morne Ronde River	SRR-3967(a)	Robertson 1992	^{14}C	135 ± 40
La Soufrière	Morne Ronde River	SRR-3967(b)	Robertson 1992	^{14}C	145 ± 40
La Soufrière 1812/1718	Proximal SE flank	C8a	Cole et al. 2019	^{14}C	146 ± 35
La Soufrière	Dry Wallibou River	SVE-089	Heath 1997	^{14}C	150 ± 40
La Soufrière	Owia	SVE-099	Heath 1997	^{14}C	155 ± 45
La Soufrière 1812/1718	Windward trail SE flank	C53	Cole et al. 2019	^{14}C	160 ± 30
La Soufrière	Wallibou River	SVE-084	Heath 1997	^{14}C	160 ± 40
La Soufrière	Dry Wallibou River	STV-106	Heath 1997	^{14}C	165 ± 45
La Soufrière 1812/1718	Proximal SE flank	C10	Cole et al. 2019	^{14}C	172 ± 37
La Soufrière	Rabacca Valley	37302	Rowley 1978	^{14}C	173 ± 50
La Soufrière	Chibarabu Point	842	Rowley 1978	^{14}C	200
La Soufrière	Wallibou sea-cliff	838	Rowley 1978	^{14}C	200
La Soufrière	Dry Wallibou	STV-366	Heath 1997	^{14}C	215 ± 45
La Soufrière	Wallibou sea-cliff	SRR-3960	Robertson 1992	^{14}C	220 ± 40
La Soufrière	Morne Ronde River	SRR-3968	Robertson 1992	^{14}C	220 ± 40
La Soufrière	Wallibou sea-cliff	SRR-3971	Robertson 1992	^{14}C	225 ± 40
La Soufrière	Morne Ronde Valley	79-56	Heath 1997	^{14}C	270 ± 45
La Soufrière 1560	Dry Wallibou valley	C2	Cole et al. 2019	^{14}C	273 ± 35
La Soufrière	Dry Wallibou River	STV-131	Heath 1997	^{14}C	290 ± 45
La Soufrière	N. Wallibou Dry River	902	Rowley 1978	^{14}C	300 ± 60
La Soufrière 1566	Dry Wallibou	C3	Cole et al. 2019	^{14}C	313 ± 35
La Soufrière	Wallibou sea-cliff	SRR-3961	Robertson 1992	^{14}C	315 ± 40
La Soufrière	N. Wallibou Dry River	901	Rowley 1978	^{14}C	320 ± 60
La Soufrière	Dry Wallibou River	SVE-095	Heath 1997	^{14}C	320 ± 45
La Soufrière	Windward Trail	STV-329	Heath 1997	^{14}C	320 ± 45
La Soufrière	Dry Wallibou River	STV-117	Heath 1997	^{14}C	330 ± 45
La Soufrière	Dry Wallibou River	SVE-088	Heath 1997	^{14}C	325 ± 45
La Soufrière	Larikai sea-cliff	SRR-3965	Robertson 1992	^{14}C	340 ± 40
La Soufrière 1590	SW coast	C5	Cole et al. 2019	^{14}C	347 ± 35

Table 4 (continued)

Volcanic centre	Location	Sample #	Reference	Method	Age (yrs BP)
La Soufrière 1551	Proximal SE flank	C11	Cole et al. 2019	^{14}C	347 ± 35
La Soufrière	Larikai sea-cliff	SRR-3964	Robertson 1992	^{14}C	390 ± 40
La Soufrière	Larikai sea-cliff	870	Rowley 1978	^{14}C	400 ± 60
La Soufrière	Wallibou sea-cliff	SRR-3959	Robertson 1992	^{14}C	405 ± 40
La Soufrière	Larikai sea-cliff	SRR-3962	Robertson 1992	^{14}C	425 ± 40
La Soufrière	Windward Trail	STV-066	Heath 1997	^{14}C	440 ± 45
La Soufrière 1445	Larakai sea-cliff	C63	Cole et al. 2019	^{14}C	450 ± 30
La Soufrière	Wallibou River	SVE-087	Heath 1997	^{14}C	465 ± 45
La Soufrière	Larikai River	37273	Rowley 1978	^{14}C	467 ± 150
La Soufrière	Larikai River	903	Rowley 1978	^{14}C	470 ± 60
La Soufrière	Windward Trail	STV-072	Heath 1997	^{14}C	475 ± 70
La Soufrière 1430	Larakai sea-cliff	C61	Cole et al. 2019	^{14}C	480 ± 30
La Soufrière	Larikai sea-cliff	SRR-3963	Robertson 1992	^{14}C	485 ± 40
La Soufrière	Larikai beach	STV-370	Heath 1997	^{14}C	490 ± 45
La Soufrière	Roseau River	SRR-3970	Robertson 1992	^{14}C	535 ± 45
La Soufrière	Wallibou sea-cliff	841	Rowley 1978	^{14}C	555 ± 70
La Soufrière	Soufrière path (E. 650 m)	843	Rowley 1978	^{14}C	615 ± 60
La Soufrière	Wallibou Dry River	840	Rowley 1978	^{14}C	635 ± 65
La Soufrière 1157	Windward trail	C8	Cole et al. 2019	^{14}C	870 ± 37
La Soufrière	Roseau River	SRR-3969	Robertson 1992	^{14}C	915 ± 45
La Soufrière	Soufrière path (E. 650 m)	844	Rowley 1978	^{14}C	1045 ± 70
La Soufrière	Mouth of Waribishy River	SVE-080	Heath 1997	^{14}C	1985 ± 40
La Soufrière	Waribishy River	STV-348	Heath 1997	^{14}C	2135 ± 40
La Soufrière	New Sandy Bay*	STV-104	Heath 1997	^{14}C	2360 ± 50
La Soufrière	Overland Village	781	Rowley 1978	^{14}C	2480 ± 70
La Soufrière	Waribishy River	778	Rowley 1978	^{14}C	2700 ± 90
La Soufrière	Rabacca Valley	37209	Rowley 1978	^{14}C	3510 ± 65
La Soufrière	Rabacca Valley	27737	Rowley 1978	^{14}C	3520 ± 70
La Soufrière	Dry Rabacca bed	STV-360	Heath 1997	^{14}C	3550 ± 45
La Soufrière	Lower Rabacca	900	Rowley 1978	^{14}C	3590 ± 70
La Soufrière	Dry Rabacca River	STV-084	Heath 1997	^{14}C	3705 ± 70
La Soufrière	Lower Rabacca	59–1	Hay 1959/Rowley 1978	^{14}C	3890 ± 300
La Soufrière	Rabacca River	STV-305a	Heath 1997	^{14}C	3925 ± 45
La Soufrière	Rabacca	845	Rowley 1978	^{14}C	3960 ± 80
La Soufrière	Rabacca Gorge	766	Rowley 1978	^{14}C	3980 ± 80
La Soufrière	Waterloo sea-cliff	SRR-3966	Robertson 1992	^{14}C	4040 ± 45
La Soufrière	Rabacca	760	Rowley 1978	^{14}C	4080 ± 60
La Soufrière	Rabacca River	59-2	Hay 1959/Rowley 1978	^{14}C	4090 ± 50
La Soufrière	Rabacca River	STV-305b	Heath 1997	^{14}C	4120 ± 45
La Soufrière	Sea-cliff, North Rabacca	777	Rowley 1978	^{14}C	4130 ± 160
La Soufrière	Rabacca Valley	846	Rowley 1978	^{14}C	4165 ± 70
La Soufrière	Rabacca Gorge	765	Rowley 1978	^{14}C	4260 ± 120
La Soufrière	Rabacca Gorge	764	Rowley 1978	^{14}C	4325 ± 95
La Soufrière	Rabacca Valley	761	Rowley 1978	^{14}C	4335 ± 95
La Soufrière	Owia*	SVE-98	Heath 1997	^{14}C	5140 ± 55
Marine Tephra					
La Soufrière	EN-46	10 cm	Carey 1992	*G. medarii* foraminifera	600 ± 600
La Soufrière	EN-46	25 cm	Carey 1992	*G. medarii* foraminifera	1600 ± 600
La Soufrière	EN-46	35 cm	Carey 1992	*G. medarii* foraminifera	2200 ± 600
La Soufrière	EN-46	40 cm	Carey 1992	*G. medarii* foraminifera	2500 ± 600

Table 4 (continued)

Volcanic centre	Location	Sample #	Reference	Method	Age (yrs BP)
La Soufrière	EN-46	50 cm	Carey 1992	*G. medarii* foraminifera	3100 ± 600
La Soufrière	GS-27	350 cm	Carey 1992	*G. medarii* foraminifera	15,000 ± 400
La Soufrière	EN-46	265 cm	Carey 1992	*G. medarii* foraminifera	15,500 ± 500
La Soufrière	GS-27	415 cm	Carey 1992	*G. medarii* foraminifera	17,600 ± 400
La Soufrière	EN-46	325 cm	Carey 1992	*G. medarii* foraminifera	18,300 ± 500
Lavas					
La Soufrière	**Lower Larikai lava**	**STV_LS_103**	**This study**	**^{40}Ar/^{39}Ar**	**4.4 ± 4.2 ka**
La Soufrière	**Crater Lava (Unit 7)**	**STV_LS_6**	**This study**	**^{40}Ar/^{39}Ar**	**5.7 ± 4.4 ka**
La Soufrière	**Crater Lava (Unit 14)**	**STV_LS_46**	**This study**	**^{40}Ar/^{39}Ar**	**7.9 ± 7.7 ka**
Morne Garu/La Soufrière	Indian Estate	STV 345	Heath 1997	^{40}Ar/^{39}Ar	11 ± 14 ka
La Soufrière	**Roseau lava**	**STV_LS_167**	**This study**	**^{40}Ar/^{39}Ar**	**14.5 ± 3.1 ka**
La Soufrière	**Crater Lava (Unit 10)**	**STV_LS_5a**	**This study**	**^{40}Ar/^{39}Ar**	**25.2 ± 3.8 ka**
La Soufrière	**Roseau lava**	**STV_LS_154**	**This study**	**^{40}Ar/^{39}Ar**	**31.5 ± 4.1 ka**
La Soufrière	**Lower Larikai lava**	**STV_LS_100**	**This study**	**^{40}Ar/^{39}Ar**	**33.7 ± 8 ka**
Morne Garu/La Soufrière	Black Point	STV 301	Heath 1997	^{40}Ar/^{39}Ar	180 ± 21 ka
La Soufrière	South Sandy Bay	STV 323	Heath 1997	^{40}Ar/^{39}Ar	291 ± 10 ka
La Soufrière	Chain Spout/Rabacca River	STV 358	Heath 1997	^{40}Ar/^{39}Ar	324 ± 15 ka
La Soufrière	Commantawana Bay	683755	Briden et al. 1979	K-Ar	360 ± 70 ka
La Soufrière*	**Jacobs well**	**VSG-2**	**This study**	**^{40}Ar/^{39}Ar**	**475.6 ± 28.3 ka**
La Soufrière	Porter Point	683740	Briden et al. 1979	K-Ar	660 ± 100 ka
La Soufrière	Rouges Hill (Owia Bay)	683756	Briden et al. 1979	K-Ar	690 ± 90 ka
Grande Bonhomme	Lowmans Leeward	683741	Briden et al. 1979	K-Ar	1.16 ± 0.08 Ma
Morne Garu	Richmond Vale	683747	Briden et al. 1979	K-Ar	1.18 ± 0.10 Ma
Grande Bonhomme	Coulls Hill	683749	Briden et al. 1979	K-Ar	1.33 ± 0.09 Ma
SE volcanics	Arnos Vale	SV-18	Geothermica Italia/Robertson 2002	K-Ar	1.54 ± 0.62 Ma
SE volcanics	Kingstown/Cane Garden road	683763	Briden et al. 1979	K-Ar	1.65 ± 0.18 Ma
SE volcanics	Villa dyke	SV-29	Geothermica Italia/Robertson 2002	K-Ar	2.50 ± 1.40 Ma
SE volcanics	Calliaqua	683762	Briden et al. 1979	K-Ar	2.49 ± 0.07 Ma
SE volcanics	Windward highway/prospect corner	683761	Briden et al. 1979	K-Ar	2.74 ± 0.11 Ma

Age in years before present (yrs BP) unless stated otherwise

Bold indicates new data presented in this study

GS-27 refers to GILLIS cruise GS7605, core 27; EN-46 refers to ENDEAVOUR cruise EN20

Sample # for marine tephra are base depths of each unit in drill core

*Xenolith

The Mafic Crater Lava (8 wt.% MgO) is a low-magnesium basalt similar in major element geochemistry to mafic tephra from the 1902/1903 eruption (Heath et al. 1998; Cole et al. 2019), a mafic pumice from the YTF (STV376; Heath et al. 1998) and two low-magnesium pre-Somma lavas (STV309 and STV315; Heath et al. 1998) (Fig. 6). The Mafic Crater Lava (Units 9 and 11; Fig. 2a) is the only effusive low-magnesium basalt to be identified within the current La Soufrière crater. Limited trace element data exist for the YTF tephra and pre-Somma lavas, but Rb, Ba, Sr, Zr and Y concentrations in the samples mentioned above generally agree within error with the Mafic Crater Lava. However, the mafic YTF tephra has higher Nb (3.7 vs 2.2 ppm) and Cr (557 vs 364 ppm) than the Mafic Crater Lava; the low-magnesium basalt pre-Somma lava STV315 has lower La (3.2 vs 4.6 ppm) and Ce (8 vs 11 ppm); and STV309 has lower V (215 vs 303 ppm) compared to the Mafic Crater Lava. Trace element data for recent pyroclastic deposits

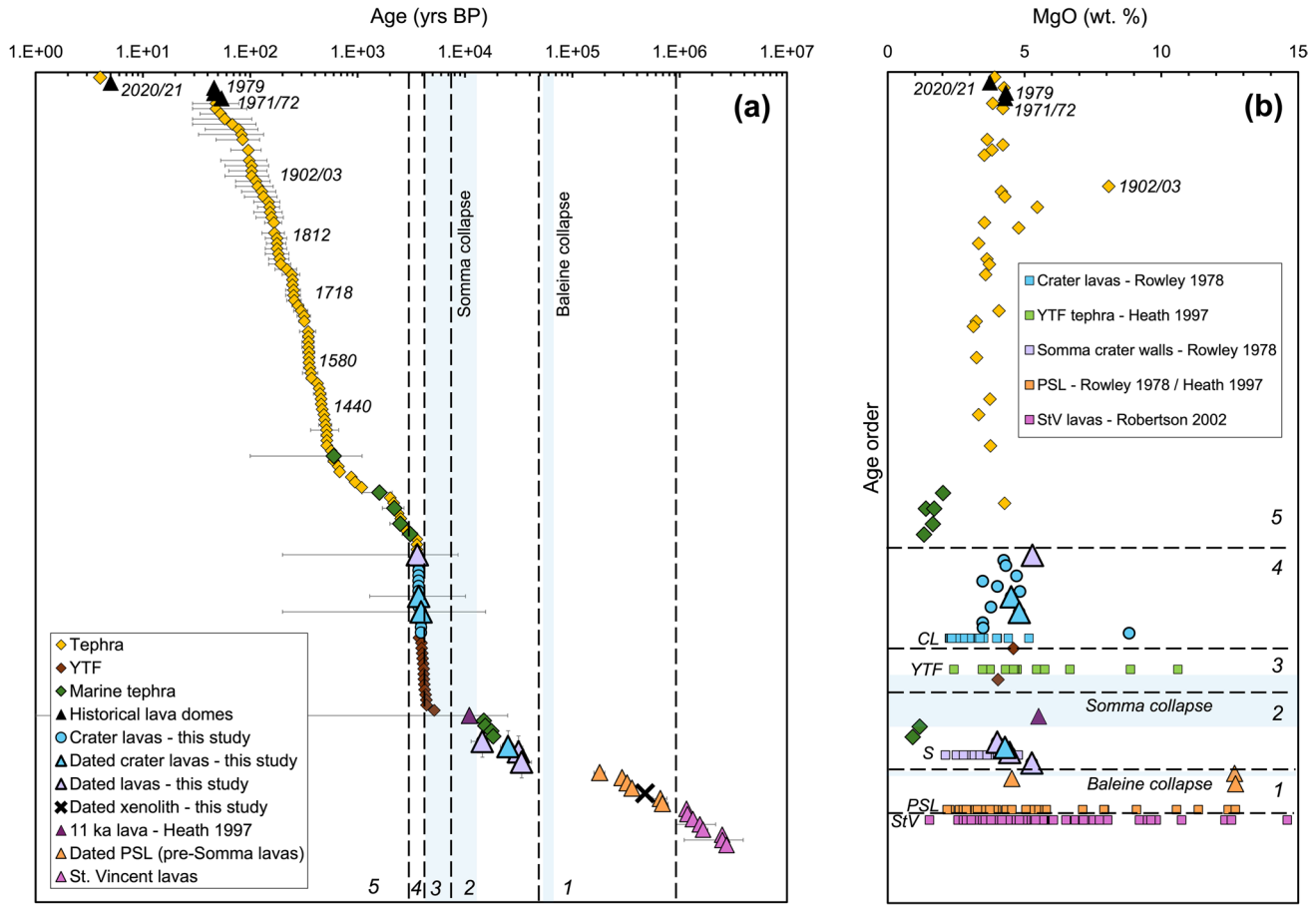

Fig. 9 **a** Stratigraphic position plotted against age (yrs BP on a log-scale). All dates are reported in Table 4, with historical eruptions labelled. Field observations confirm the younger Crater Lavas overlie the YTF (Sigurdsson 1981); hence, they are plotted at younger than their calculated average age, but still within error of their $^{40}Ar/^{39}Ar$ ages. Radiocarbon dating of tephra samples extends back to ~ 5 ka (Rowley 1978; Robertson, 1992; Heath 1997; Cole et al. 2019). Marine tephra in drill cores GS-27 and EN-46 in the Grenada basin were correlated to St. Vincent using geochemical fingerprinting (Carey 1992) and dated using sedimentation rates and the disappearance of planktonic foraminifera in the *Globorotalia medarii* complex at the end of the last ice age (12 ka; Sigurdsson and Carey 1981; Reid et al. 1996). Table 4 lists the depths of the St. Vincent units in these drill cores and their corresponding ages (0.6–18 ka). K-Ar and $^{40}Ar/^{39}Ar$ dating of pre-Somma lavas collected from the flanks of the volcano range from 690 to 180 ka (Briden et al. 1979; Heath 1997) and K-Ar ages of older St. Vincent lavas extend back from 1.16 to 2.74 Ma (Briden et al. 1979; Robertson 2002). Dashed lines define the different stages of La Soufrière's eruptive history: 1, pre-Somma lavas; 2, Somma lavas; 3, Yellow Tuff Formation; 4, Crater Lavas; 5, Pyroclastic Formation. Blue shading represents possible periods of edifice collapse. The date of the Somma collapse is unknown but is bounded by the youngest dated Somma lava and YTF eruption. The Somma collapse and YTF are tentatively linked based on observations in the south crater wall (Sigurdsson 1981). The dated xenolith (VSG-2) sits with the pre-Somma lavas. **b** Stratigraphic position plotted against MgO (wt.%) to show compositional variation over time. Whole-rock compositions of dated lavas and tephra (containing radiocarbon dated charcoal). Note marine tephra are glasses not whole-rock and hence lower MgO. Symbols, dashed lines and shading as in **a**. Compositions of units that were not dated but whose relative position known are shown as squares with their colour and label correlating to volcanic period to display the full chemical diversity at La Soufrière. Abbreviations as in Fig. 5, as well as S - Somma lavas and StV - St. Vincent lavas from older volcanic centres

(Cole et al. 2019) show the mafic 1902/1903 tephra are in very good agreement with the Mafic Crater Lava trace element concentrations but are slightly elevated in LREE (e.g. 5.5 vs 4.6 ppm La) and vary in V and Cr concentrations. Cr, however, notably varies within the Mafic Crater Lava samples by ~ 90 ppm, possibly reflecting Cr-spinel fractionation or other Cr-rich mineral phases such as olivine and clinopyroxene (Barnes and Roeder 2001). In general, the low-magnesium basalts of La Soufrière are compositionally very similar over a wide time interval suggesting they could be sourced from similar physio-chemical conditions in the crust.

Previous studies (e.g. Heath et al. 1998) suggest more primitive volcanism decreased and eventually ceased over time at La Soufrière. Although the pre-Somma lavas show similar chemical variations to earlier volcanic centres on

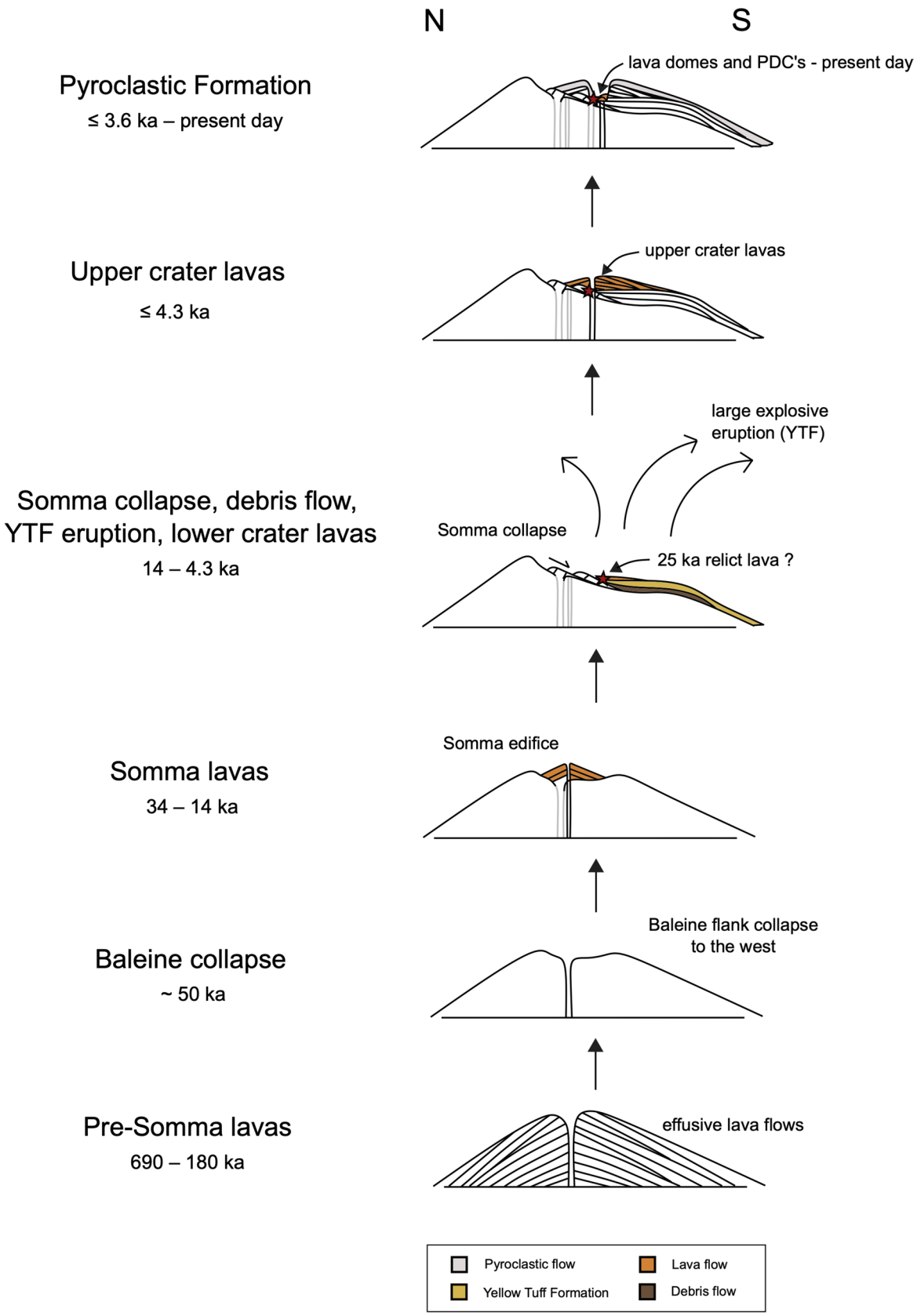
N
S
Pyroclastic Formation
≤ 3.6 ka – present day
lava domes and PDC's - present day
Upper crater lavas
≤ 4.3 ka
upper crater lavas
Somma collapse, debris flow,
YTF eruption, lower crater lavas
14 – 4.3 ka
large explosive
eruption (YTF)
Somma collapse
25 ka relict lava ?
Somma lavas
34 – 14 ka
Somma edifice
Baleine collapse
~ 50 ka
Baleine flank collapse
to the west
Pre-Somma lavas
690 – 180 ka
effusive lava flows
Pyroclastic flow
Lava flow
Yellow Tuff Formation
Debris flow

◂**Fig. 10** Schematic of revised eruptive history at La Soufrière. Pre-Somma lavas date back to 690 ± 90 ka (Briden et al. 1979). The Baleine collapse is estimated at 50 ka (Le Friant et al. 2009), followed by the extrusion of the Somma lavas. A lower Larikai valley lava dated at 33.7 ± 8.0 ka and Roseau lava dated at 14.5 ± 3.1 ka represent the oldest and youngest dated lavas of the Somma period. Collapse of the Somma edifice to the south generated voluminous debris flows and parts of the crater walls may have slumped into the crater (e.g. 25.2 ± 3.8 ka crater lava depicted by a red star). The Somma collapse is also linked to the large explosive YTF eruption and possible outpourings of lava (Sigurdsson 1981). A lava flow in the lower Larikai valley is dated at 4.4 ± 4.2 ka. Radiogenic dates of overlying pyroclastic deposits constrain the YTF eruption to before 3.6 ka (Rowley 1978). The Crater Lavas overlie the YTF deposits in the crater; therefore, they must be younger (Sigurdsson 1981). New $^{40}Ar/^{39}Ar$ dates have large uncertainty but give ages of 7.9 ± 7.7 ka and 5.7 ± 4.4 ka for the upper crater lavas. The maximum age of the YTF is therefore constrained by the youngest Somma lava at 14.5 ± 3.1 ka. The Pyroclastic Formation incorporates all volcanism after the Crater Lavas and YTF eruption including present day eruptions. Today, explosive eruptions excavate new craters and deposit thick pyroclastic units whilst effusive volcanism is restricted to within the crater.

St. Vincent, it is possible that the high-magnesium basalts, attributed to the pre-Somma stage (orange squares and triangles with ≥ 10 wt.% MgO; Fig. 9b), may instead be lava flows from Morne Garu volcanic centre (Fig. 1b) upon which La Soufrière grew. Lavas from the Somma crater walls (lilac squares Fig. 9b; Rowley 1978) are geochemically similar to the lavas presented in this study (except the Mafic Crater Lava) and previously sampled La Soufrière crater lavas, suggesting the magmatic system had homogenised by the time the Somma edifice grew. One hypothesis is that the large flank collapse eruption that formed the Baleine scarp could have resulted in major changes in the magma plumbing system and subsequent stabilisation of erupted magma compositions as observed on Montserrat (Cassidy et al. 2015), St. Eustatius (Roobol and Smith 2004) and St. Lucia (Boudon et al. 2013). There is however a period of 146 kyr that remains unaccounted for, during which the Baleine collapse occurred, and where the variation of magma compositions (if erupted) is unknown.

Five of the lava blocks recovered from the YTF are geochemically distinct, with elevated CaO and Al_2O_3 and lower SiO_2 and Na_2O than other La Soufrière lavas (Fig. 6). Two of these blocks (STV_LS_22 and 24) also have high Sr (Fig. 7). Elevated Sr and Ca have previously been associated with two different magma types, M- and C-series, in Grenada and the Grenadines (Stamper et al. 2014; White et al. 2017; Melekhova et al., 2022). High-Ca magmas have not previously been reported at St. Vincent but are observed in the melt inclusion record (Fig. 6), supporting the presence of Ca-rich melts in the subsurface. The chemically anomalous lava blocks in the highly explosive YTF eruption may derive from a previously unsampled part of the La Soufrière magmatic system mobilised by the Somma collapse.

Hornblende-gabbro xenolith

The hornblende-gabbro xenolith dated in this study corresponds in age to the pre-Somma stage at 476 ka (Fig. 9a), suggesting it represents a fragment of the sub-volcanic crystal mush that was active at the time. Erupted melts may either have been extracted from these mushes or passed through them en route to the surface. The presence of hornblende in the gabbroic xenolith is consistent with trace element evidence for amphibole fractionation for all analysed St. Vincent magmas (Fig. 8b), despite the total absence of hornblende as a phenocryst or microlite phase. This observation requires a significant volume of amphibole-bearing mush at depths below the arc; the 'amphibole sponge' of Davidson et al. (2007).

Recently identified micro-xenoliths in erupted scoria samples from historic and pre-historic La Soufrière have gabbroic mineral assemblages containing abundant orthopyroxene, but lacking amphibole and olivine (Fedele et al. 2021), suggesting compositional change in the underlying mush over time, such that micro-xenoliths represent the currently active system, or sections of the mush not previously sampled. Melekhova et al. (2019) have shown that the mineralogy of plutonic xenoliths in the Lesser Antilles is controlled by P-T-H_2O-fO_2 conditions in the subsurface. Thus, changes in magma source depths and temperatures over time may be reflected in changes in xenolith mineralogy. What is clear, however, is that the explosive and effusive phases have near-constant chemistry for almost 4 kyr (Fig. 9b), suggestive of sourcing from a stable, chemically buffered magma reservoir at depth (e.g. Blundy 2022).

Conclusions

New $^{40}Ar/^{39}Ar$ ages for lavas erupted from La Soufrière fill a gap in the eruptive history record and reveal four key findings. First, we have obtained radiometric ages for the previously unconstrained Somma stage (34–14 ka). These lavas narrow the major gap in the stratigraphic sequence to between 34 and 180 ka, which straddles the postulated age of the Baleine collapse (~ 50 ka). The two lavas dated around 34 ka from the lower Larikai and Roseau valleys likely mark the onset of renewed volcanism following collapse. Second, a pronounced unconformity is identified in the northern wall of the current crater where the oldest crater lava (25.2 ± 3.8 ka) is overlain by crater lavas that are considerably younger (7.9 ± 7.7 and 5.7 ± 4.4 ka) and coeval with the YTF. The anomalously old crater lava, described as a 'pre-historic coulee' by Sigurdsson (1981), is considered to represent a vestigial part of the Somma crater that survived the Somma collapse or even a slumped lava block of Somma lava. Third, dates for lavas exposed

on the western flanks of La Soufrière range from 33.7 ± 8 to 4.4 ± 4.2 ka thus corresponding to both Crater Lava and Somma stages. The youngest lava flow in the lower Larikai valley is crosscut by a dyke, suggesting volcanism on the western flank of La Soufrière continued until more recently than previously thought, possibly coeval with the emplacement of the youngest Crater Lavas. Subsequent effusive volcanism produced lava domes confined to the crater. Finally, we have dated, for the first time, an erupted plutonic xenolith from La Soufrière. The age of 475.6 ± 28.3 ka is in agreement with early pre-Somma magmatism. The xenolith could represent a fragment of underlying crystal mush that is no longer active.

Based on our new age determinations and revised stratigraphy, we have identified five key stages in the magmatic history of La Soufriere: pre-Somma, Somma, Yellow Tuff Formation, Crater Lavas and Pyroclastic Formation (including historic eruptions). The pre-Somma and Somma stages are separated by the Baleine collapse; the Somma collapse and associated debris flow immediately pre-date the YTF. Arguably, the YTF could be ascribed to a terminal Somma stage or an embryonic Crater Lavas stage; hence, we assign it its own stage.

We show that magmas erupted from La Soufrière over the last 34 kyr are predominantly basaltic andesite with very limited major and trace element chemical variation in contrast to more compositionally diverse magmas of the pre-Somma stage and elsewhere on St. Vincent. Elevated REE concentrations and trace element ratios indicate that the post-34-ka magmas experienced a small degree of differentiation relative to each other, fractionating plagioclase and amphibole at hydrous and oxidising conditions. These observations agree with previous experimental studies that found basaltic andesite magmas on St. Vincent to be generated by polybaric differentiation at lower crustal conditions from a mantle-derived, high-magnesium basalt parent (Melekhova et al. 2015). Trace element ratios suggest low sediment or crustal input into the magmas.

A low-magnesium basaltic crater lava (~ 8 wt.% MgO) is identified that is more primitive than all other crater lavas and is the oldest representative of the Crater Lavas stage. This Mafic Crater Lava is geochemically similar to a small number of previously reported mafic tephra in the YTF and 1902/1903 deposits and low-magnesium basaltic pre-Somma lavas. These rare mafic pyroclastic products correlate with two of the largest explosive eruptions at La Soufrière (YTF and 1902/1903). Collapse of the Somma edifice could have triggered the YTF eruption by rapid depressurisation of the magmatic system. Such large-scale eruptions can result in deeper, more primitive (and perhaps more diverse) magma sources being tapped (Manconi et al. 2009), as was observed in the 1902/1903 eruption (Roobol and Smith 1975).

The compositional monotony of La Soufrière basaltic andesite magmas is suggestive of a long-lived, chemically buffered source region, whose mineralogy corresponds to that of erupted plutonic xenoliths. Reactions between the mush and interstitial melts may have provided this buffering, as envisaged by Blundy (2022). Less-evolved, low-magnesium basalt magmas may occur locally within the source region but only become liberated and erupted during major perturbations to the systems, such as the two well-documented collapse events or major explosive eruptions, such as that in 1902/1903.

Appendix

Extended methods

Rock powder preparation

Rock powder preparation for all samples collected in this study was performed at the University of Oxford. Lava samples were initially split into smaller fragments (≤ 5 cm3) and any alteration removed using a stainless-steel rock splitter. Samples were then washed in an ultrasonic bath for 10 min and left to dry overnight in a 40 °C oven. Approximately 200 g of the clean sample material was crushed to ≤ 1 mm using a jaw crusher, where a stainless-steel fixed-jaw and removable-jaw crush the material in 1-mm intervals, from 5 to ≤ 1 mm. The crushed material was then poured through a stainless-steel sample splitter at least three times to ensure a homogenous and representative batch of material.

Grinding of sample material to a fine powder was carried out using either the agate ball mill or Tema mill. The ball mill contains four agate holders, each containing 10 agate balls, allowing four samples to be powdered simultaneously. Forty grams of sample material was weighed into each agate holder and run at 400 rpm for 20 min. The Tema mill contains an inner and outer agate ring. Again, 40 g of sample material was added to the agate container and run for 10–20 min until a fine powder was obtained. Approximately 10 g of each rock powder was weighed into a glass vial and sent to ALS Geochemistry, Loughrea, Ireland, for whole-rock major and trace element analysis.

All equipment was cleaned with compressed air and ethanol between each sample. The mills were also run with cleaning silica between samples to reduce contamination.

U5 scoria preparation

Trace elements of the U5 scoria bulk rock were prepared and analysed at Union College. For each analysis, 200 mg of powdered sample was weighed into a PicoTrace (Bovendan, Germany) Teflon bomb system. Four standards were

used for calibration. The powders were dissolved through several steps. Rock powders were dissolved in 0.5 mL of 50% HF and heated to 180 °C for 4 days and then allowed to cool and evaporate at 100 °C. Fifteen milliliters of 70% HNO3 was then added and allowed to evaporate again. A mixture of 125 mL HNO3, 25 mL of 37% HCl, 2 mL of HF and 0.3 mL of 1000 ng/g internal standards including Rh, In, Re and Bi was diluted to 500 mL and 15 mL added to each sample. The Teflon crucibles were sealed and heated to 150 °C overnight. Once cooled, 0.2 mL of each sample solution and 10 mL of 1% HNO3 were added to 12-mL test tubes for analysis.

Dilute samples were analysed on an Agilent 8900 ICP-QQQ Triple-Quad Mass Spectrometer in No-Gas mode for the lightest and heaviest elements (Li, Be, Pb, Th, U), in O2 gas mode for V, Cr, Co, Sb and REEs and in He gas mode for all others. Powdered natural reference materials from 3 basalts and 1 rhyolite, NIST (688, 278) and the USGS (BIR-1, BCR-2) were used for standardisation. To check method accuracy, USGS basalt standard BHVO-2 was run as an unknown, and measured compositions match known values within 5% for all elements, with the exception of Mo, Sn and Sb which are generally within

Unsuccessful $^{40}Ar/^{39}Ar$ dates

One crater lava (STV_LS_11; Unit 4) close to the top of the crater lava sequence gave a negative age due to its recent eruption and high 36Ar content (likely ≤ 4 ka). Crater lava STV_LS_3 (Unit 1) sits stratigraphically above STV_LS_11, so it was not dated. The Upper Larikai dyke gave a staircase-upwards plateau spectrum indicative of excess 40Ar (Schaen et al., 2020).

Supplementary Information The online version contains supplementary material available at https://doi.org/10.1007/s00445-026-01964-y.

Acknowledgements We thank the Royal Society for providing funding for a DPhil studentship to BME and a Research Professorship to JB (RP\R1\201048), and a University Research Fellowship to GC (URF\R1\221161). University College Oxford kindly provided part of the funding for BME's fieldwork. We thank Michal Camejo-Harry, Monique Johnson, Tyrone Stafford and Megan Taylor for help during fieldwork; Steve Carey for providing the marine tephra dates; and Paul Cole for insightful discussions. Thank you to our reviewers for providing helpful comments and suggestions, and Marie Edmonds for editorial handling.

Author contributions Conceptualisation: [EM, RR, JB, BM-E]; Methodology: [BM-E, EM, JB]; Investigation [BM E, EM, GC, RR]; Formal analysis: [BM-E, BJ, HF]; Writing - original draft preparation: [BM E]; Writing - review and editing: [BME, JB, EM, GC, RR, BJ, HF]; Visualisation [BM-E]; Funding acquisition: [JB, GC]; Supervision: [JB, EM].

Funding This work was supported by the Royal Society (RP\R1\201048 and URF\R1\221161). University College, Oxford, provided additional funding for fieldwork.

Data Availability No datasets were generated or analysed during the current study.

Declarations

Competing interests The authors declare no competing interests.

References

Aigner-Torres M, Blundy J, Ulmer P, Pettke T (2007) Laser ablation ICPMS study of trace element partitioning between plagioclase and basaltic melts: an experimental approach. Contrib Mineral Petrol 153:647–667. https://doi.org/10.1007/s00410-006-0168-2

Arculus RJ, Wills KJA (1980) The petrology of plutonic blocks and inclusions from the Lesser Antilles Island Arc. J Petrol 21:743–799. https://doi.org/10.1093/petrology/21.4.743

Atlas ZD, Germa A, Boss B et al (2022) Variable element enrichment sources and contributions to volcanic rocks along the Lesser Antilles Island Arc. Front Earth Sci 10:782179. https://doi.org/10.3389/feart.2022.782179

Bardintzeff JM (1983) Les verres et les magmas de l'eruption 1979 de la Soufriere de Saint-Vincent (Antilles). Bull Soc Geol Fr 7:811–818. https://doi.org/10.2113/gssgfbull.S7-XXV.6.811

Bardintzeff J-M (1984) Les pyroxènes et leurs inclusions, marqueurs privilégiés des nuées ardentes (Saint-Vincent, Antilles, 1979). Bulmi 107:41–54. https://doi.org/10.3406/bulmi.1984.7792

Barnes SJ, Roeder PL (2001) The range of spinel compositions in terrestrial mafic and ultramafic rocks. J Petrol 42:2279–2302. https://doi.org/10.1093/petrology/42.12.2279

Blundy J (2022) Chemical differentiation by mineralogical buffering in crustal hot zones. J Petrol 63:egac054. https://doi.org/10.1093/petrology/egac054

Boudon G, Villemant B, Friant AL et al (2013) Role of large flank-collapse events on magma evolution of volcanoes. Insights from the Lesser Antilles Arc. J Volcanol Geotherm Res 263:224–237. https://doi.org/10.1016/j.jvolgeores.2013.03.009

Bouvier A-S, Métrich N, Deloule E (2008) Slab-derived fluids in the magma sources of St. Vincent (Lesser Antilles Arc): volatile and light element imprints. J Petrol 49:1427–1448. https://doi.org/10.1093/petrology/egn031

Briden JC, Rex DC, Faller AM, Tomblin JF (1979) K-Ar geochronology and palaeomagnetism of volcanic rocks in the Lesser Antilles island arc. Phil Trans R Soc Lond A 291:485–528. https://doi.org/10.1098/rsta.1979.0040

Brown GM, Holland JG, Sigurdsson H et al (1977) Geochemistry of the Lesser Antilles volcanic island arc. Geochim Cosmochim

Acta 41:785–801. https://doi.org/10.1016/0016-7037(77)90049-7
Brown JR, Cooper GF, Humphreys MCS et al (2026) Plutonic xenoliths reveal the influence of cryptic melt-mush reaction processes in the plumbing system beneath St Vincent, Lesser Antilles Arc. J Petrol. https://doi.org/10.1093/petrology/egag014
Camejo-Harry M, Melekhova E, Aufrère S et al (2024) Early arc crust formation preserved in the Grenadines archipelago, southern Lesser Antilles arc. R Soc Open Sci 11:231914. https://doi.org/10.1098/rsos.231914
Carey S (1992) Studies on the generation, dispersal and deposition of tephra in the marine and terrestrial environment. PhD Thesis, Universiry of Rhode Island
Cassidy M, Cole P, Hicks KE et al (2015) Rapid and slow: varying magma ascent rates as a mechanism for Vulcanian explosions. Earth Planet Sci Lett 420:73–84. https://doi.org/10.1016/j.epsl.2015.03.025
Cassidy M, Manga M, Cashman K, Bachmann O (2018) Controls on explosive-effusive volcanic eruption styles. Nat Commun 9:2839. https://doi.org/10.1038/s41467-018-05293-3
Churikova T, Dorendorf F, Wörner G (2001) Sources and fluids in the Mantle Wedge below Kamchatka, evidence from across-arc geochemical variation. J Petrol 42:1567–1593. https://doi.org/10.1093/petrology/42.8.1567
Cole PD, Robertson REA, Fedele L, Scarpati C (2019) Explosive activity of the last 1000 years at La Soufrière, St Vincent, Lesser Antilles. J Volcanol Geotherm Res 371:86–100. https://doi.org/10.1016/j.jvolgeores.2019.01.002
Cole PD, Barclay J, Robertson REA et al (2024) Explosive sequence of La Soufrière, St Vincent, April 2021: insights into drivers and consequences via eruptive products. SP 539:81–106. https://doi.org/10.1144/SP539-2022-292
Cooper GF, Macpherson CG, Blundy JD et al (2020) Variable water input controls evolution of the Lesser Antilles volcanic arc. Nature 582:525–529. https://doi.org/10.1038/s41586-020-2407-5
Davidson J, Turner S, Handley H et al (2007) Amphibole "sponge" in arc crust? Geology 35:787. https://doi.org/10.1130/G23637A.1
Davidson J, Turner S, Plank T (2013) Dy/Dy*: variations arising from mantle sources and petrogenetic processes. J Petrol 54:525–537. https://doi.org/10.1093/petrology/egs076
Devine JD, Sigurdsson H (1980) Garnet–fassaite calc-silicate nodule from La Soufrière, St. Vincent. Am Mineral 65:302–305
Dostal J, Dupuy C, Carron JP et al (1983) Partition coefficients of trace elements: application to volcanic rocks of St. Vincent, West Indies. Geochim Cosmochim Acta 47:525–533. https://doi.org/10.1016/0016-7037(83)90275-2
Elliott T (2003) Tracers of the slab. In: Eiler J (ed) Geophysical Monograph Series. American Geophysical Union, Washington, D. C., pp 23–45
Fedele L, Cole PD, Scarpati C, Robertson REA (2021) Petrological insights on the last 1000 years of explosive activity at La Soufrière volcano, St. Vincent (Lesser Antilles). Lithos 392:106150. https://doi.org/10.1016/j.lithos.2021.106150
Graham AM, Thirlwall MF (1981) Petrology of the 1979 eruption of Soufriere volcano, St. Vincent, Lesser Antilles
Hawkesworth CJ, Hergt J, Ellam R, McDermott F (1991) Element fluxes associated with subduction related magmatism. Phil Trans R Soc Lond A 335:393–405. https://doi.org/10.1098/rsta.1991.0054
Heath E (1997) Genesis and evolution of calc-alkaline magmas at Soufriere volcano, St. Vincent, Lesser Antilles arc. PhD Thesis, Lancaster University
Heath E, Macdonald R, Belkin H et al (1998) Magmagenesis at Soufriere Volcano, St Vincent, Lesser Antilles Arc. J Petrol 39:1721–1764. https://doi.org/10.1093/petroj/39.10.1721
Hildreth W, Moorbath S (1988) Crustal contributions to arc magmatism in the Andes of Central Chile. Contrib Mineral Petrol 98:455–489. https://doi.org/10.1007/BF00372365
Jicha BR, Singer BS, Sobol P (2016) Re-evaluation of the ages of 40Ar/39Ar sanidine standards and supereruptions in the western U.S. using a Noblesse multi-collector mass spectrometer. Chem Geol 431:54–66. https://doi.org/10.1016/j.chemgeo.2016.03.024
Koleszar AM, Kent AJR, Wallace PJ, Scott WE (2012) Controls on long-term low explosivity at andesitic arc volcanoes: insights from Mount Hood, Oregon. J Volcanol Geotherm Res 219–220:1–14. https://doi.org/10.1016/j.jvolgeores.2012.01.003
Koulakov I, Abkadyrov I, Al Arifi N et al (2017) Three different types of plumbing system beneath the neighboring active volcanoes of Tolbachik, Bezymianny, and Klyuchevskoy in Kamchatka. J Geophys Res Solid Earth 122:3852–3874. https://doi.org/10.1002/2017JB014082
Lacroix A (1949) Sur des enclaves endopolygènes de Saint-Vincent. Bulmi 72:571–590. https://doi.org/10.3406/bulmi.1949.4686
Le Bas MJ, Maitre RWL, Streckeisen A et al (1986) A chemical classification of volcanic rocks based on the total alkali-silica diagram. J Petrol 27:745–750. https://doi.org/10.1093/petrology/27.3.745
Le Friant A, Boudon G, Arnulf A, Robertson REA (2009) Debris avalanche deposits offshore St. Vincent (West Indies): impact of flank-collapse events on the morphological evolution of the island. J Volcanol Geotherm Res 179:1–10. https://doi.org/10.1016/j.jvolgeores.2008.09.022
Lee J-Y, Marti K, Severinghaus JP et al (2006) A redetermination of the isotopic abundances of atmospheric Ar. Geochim Cosmochim Acta 70:4507–4512. https://doi.org/10.1016/j.gca.2006.06.1563
Lewis JF (1973) Petrology of the ejected plutonic blocks of the Soufriere volcano, St. Vincent, West Indies. J Petrol Geol 14:81–112
Maccaferri F, Richter N, Walter TR (2017) The effect of giant lateral collapses on magma pathways and the location of volcanism. Nat Commun 8:1097. https://doi.org/10.1038/s41467-017-01256-2
Macdonald R, Hawkesworth CJ, Heath E (2000) The lesser Antilles volcanic chain: a study in arc magmatism. Earth-Sci Rev 49:1–76. https://doi.org/10.1016/S0012-8252(99)00069-0
Manconi A, Longpre M-A, Walter TR et al (2009) The effects of flank collapses on volcano plumbing systems. Geology 37:1099–1102. https://doi.org/10.1130/G30104A.1
Melekhova E, Blundy J, Robertson R, Humphreys MCS (2015) Experimental evidence for polybaric differentiation of primitive arc basalt beneath St. Vincent, Lesser Antilles. J Petrol Geol 56:161–192. https://doi.org/10.1093/petrology/egu074
Melekhova E, Blundy J, Martin R et al (2017) Petrological and experimental evidence for differentiation of water-rich magmas beneath St. Kitts, Lesser Antilles. Contrib Mineral Petrol 172:98. https://doi.org/10.1007/s00410-017-1416-3
Melekhova E, Schlaphorst D, Blundy J et al (2019) Lateral variation in crustal structure along the Lesser Antilles arc from petrology of crustal xenoliths and seismic receiver functions. Earth Planet Sci Lett 516:12–24. https://doi.org/10.1016/j.epsl.2019.03.030
Min K, Mundil R, Renne PR, Ludwig KR (2000) A test for systematic errors in 40Ar/39Ar geochronology through comparison with U/Pb analysis of a 1.1-Ga rhyolite. Geochim Cosmochim Acta 64:73–98. https://doi.org/10.1016/S0016-7037(99)00204-5
Mixon EE, Singer BS, Jicha BR, Ramirez A (2021) Calbuco, a monotonous andesitic high-flux volcano in the Southern Andes, Chile. J Volcanol Geotherm Res 416:107279. https://doi.org/10.1016/j.jvolgeores.2021.107279
Nakamura N (1974) Determination of REE, Ba, Fe, Mg, Na and K in carbonaceous and ordinary chondrites. Geochim Cosmochim Acta 38:757–775. https://doi.org/10.1016/0016-7037(74)90149-5
Parat F, Streck MJ, Holtz F, Almeev R (2014) Experimental study into the petrogenesis of crystal-rich basaltic to andesitic magmas at

Arenal volcano. Contrib Mineral Petrol 168:1040. https://doi.org/10.1007/s00410-014-1040-4
Pichavant M, Macdonald R (2007) Crystallization of primitive basaltic magmas at crustal pressures and genesis of the calc-alkaline igneous suite: experimental evidence from St Vincent, Lesser Antilles arc. Contrib Mineral Petrol 154:535–558. https://doi.org/10.1007/s00410-007-0208-6
Pichavant M, Mysen BO, Macdonald R (2002) Source and H_2O content of high-MgO magmas in island arc settings: an experimental study of a primitive calc-alkaline basalt from St. Vincent, lesser antilles arc. Geochim Cosmochim Acta 66:2193–2209. https://doi.org/10.1016/S0016-7037(01)00891-2
Plank T (2005) Constraints from thorium/lanthanum on sediment recycling at subduction zones and the evolution of the continents. J Petrol 46:921–944. https://doi.org/10.1093/petrology/egi005
Plank T, Langmuir CH (1993) Tracing trace elements from sediment input to volcanic output at subduction zones. Nature 362:739–743. https://doi.org/10.1038/362739a0
Powell R, Hergt J, Woodhead J (2002) Improving isochron calculations with robust statistics and the bootstrap. Chem Geol 185:191–204. https://doi.org/10.1016/S0009-2541(01)00403-X
Pushkar P, Steuber AM, Tomblin JF, Julian GM (1973) Strontium isotopic ratios in volcanic rocks from St. Vincent and St. Lucia, Lesser Antilles. J Geophys Res 78:1279–1287. https://doi.org/10.1029/JB078i008p01279
Reid R, Carey SN, Ross DR (1996) Late quaternary sedimentation in the Lesser Antilles island arc. Geol Soc Am Bull 108:78–100. https://doi.org/10.1130/0016-7606(1996)108%3c0078:LQSITL%3e2.3.CO;2
Robertson R (2002) The volcanic geology of the pre-Soufrière rocks of St. Vincent, West Indies. PhD Thesis, University of the West Indies
Robertson REA (2005) Volcanic hazard atlas of the Lesser Antilles: St. Vincent. Volcanic hazard atlas of the Lesser Antilles. Seismic Research Unit, The University of the West Indies, Trinidad and Tobago, pp 239–261
Roobol MJ, Smith AL (1975) A comparison of the recent eruptions of Mt. Pelee, Martinique and Soufriere, St. Vincent
Roobol MJ, Smith AL (2004) Volcanology of Saba and St. Eustatius northern lesser Antilles. Royal Netherlands Academy of Arts and Sciences (Koninklijke Nederlandse Akademie Van Wetenschappen)
Rowley K (1978) Stratigraphy and geochemistry of the Soufriere volcano, St. Vincent, West Indies. PhD Thesis, University of the West Indies St. Augustine - Seismic Research Unit
Schmidt ME, Grunder AL (2011) Deep mafic roots to arc volcanoes: mafic recharge and differentiation of basaltic andesite at North Sister Volcano, Oregon Cascades. J Petrol 52:603–641. https://doi.org/10.1093/petrology/egq094
Sigurdsson H (1981) Geologic observations in the crater of Soufrière volcano, St. Vincent. University of the West Indies, Seismic Research Unit, Special Publication 1981/1.
Sigurdsson H, Carey SN (1981) Marine tephrochronology and quaternary explosive volcanism in the Lesser Antilles Arc. In: Self S, Sparks RSJ (eds) Tephra Studies. Springer, Netherlands, Dordrecht, pp 255–280
Sisson TW, Salters VJM, Larson PB (2014) Petrogenesis of Mount Rainier andesite: magma flux and geologic controls on the contrasting differentiation styles at stratovolcanoes of the southern Washington Cascades. Geol Soc Am Bull 126:122–144. https://doi.org/10.1130/B30852.1
Stamper CC, Blundy JD, Arculus RJ, Melekhova E (2014) Petrology of plutonic xenoliths and volcanic rocks from Grenada, Lesser Antilles. J Petrol 55:1353–1387. https://doi.org/10.1093/petrology/egu027
Streck MJ, Dungan MA, Malavassi E et al (2002) The role of basalt replenishment in the generation of basaltic andesites of the ongoing activity at Arenal volcano, Costa Rica: evidence from clinopyroxene and spinel. Bull Volcanol 64:316–327. https://doi.org/10.1007/s00445-002-0209-2
Streck MJ, Dungan MA, Bussy F, Malavassi E (2005) Mineral inventory of continuously erupting basaltic andesites at Arenal volcano, Costa Rica: implications for interpreting monotonous, crystal-rich, mafic arc stratigraphies. J Volcanol Geotherm Res 140:133–155. https://doi.org/10.1016/j.jvolgeores.2004.07.018
Sun S, McDonough WF (1989) Chemical and isotopic systematics of oceanic basalts: implications for mantle composition and processes. SP 42:313–345. https://doi.org/10.1144/GSL.SP.1989.042.01.19
Tang M, Ji W-Q, Chu X et al (2021) Reconstructing crustal thickness evolution from europium anomalies in detrital zircons. Geology 49:76–80. https://doi.org/10.1130/G47745.1
Tatsumi Y, Furukawa Y, Yamashita S (1994) Thermal and geochemical evolution of the mantle wedge in the northeast Japan arc: 1. Contribution from experimental petrology. J Geophys Res 99:22275–22283. https://doi.org/10.1029/94JB00283
Thirlwall MF, Smith TE, Graham AM et al (1994) High field strength element anomalies in arc lavas: source or process? J Petrol 35:819–838. https://doi.org/10.1093/petrology/35.3.819
Tollan PME, Bindeman I, Blundy JD (2012) Cumulate xenoliths from St. Vincent, Lesser Antilles Island Arc: a window into upper crustal differentiation of mantle-derived basalts. Contrib Mineral Petrol 163:189–208. https://doi.org/10.1007/s00410-011-0665-9
Turner SJ, Langmuir CH (2022) Sediment and ocean crust both melt at subduction zones. Earth Planet Sci Lett 584:117424. https://doi.org/10.1016/j.epsl.2022.117424
Wager LR (1962) Igneous cumulates from the 1902 eruption of Soufriere, St. Vincent. Bull Volcanol 24:93–99
Weber G, Blundy J, Barclay J et al (2024) Petrology of the 2020–21 effusive to explosive eruption of La Soufrière Volcano, St Vincent: insights into plumbing system architecture and magma assembly mechanism. SP 539:171–200. https://doi.org/10.1144/SP539-2022-177
White W, Copeland P, Gravatt DR, Devine JD (2017) Geochemistry and geochronology of Grenada and Union islands, Lesser Antilles: the case for mixing between two magma series generated from distinct sources. Geosphere 13:1359–1391. https://doi.org/10.1130/GES01414.1